HOLLOW PLUME MITIGATION OF A HIGH-EFFICIENCY MULTISTAGE PLASMA THRUSTER

A Thesis

Presented to

the Faculty of California Polytechnic State University

San Luis Obispo

In Partial Fulfillment

of the Requirements for the Degree

Master of Science in Aerospace Engineering

by

Scott A. McGrail

December 2013

COMMITTEE MEMBERSHIP

TITLE:	Hollow Plume Mitigation of a High-Efficiency Multistage Plasma Thruster
AUTHOR:	Scott A. McGrail
DATE SUBMITTED:	December 2013
COMMITTEE CHAIR:	Kira Abercromby, Ph.D, Assistant Professor of Aerospace Engineering
COMMITTEE MEMBER:	Dan Goebel, Ph.D, Senior Research Scientist at Jet Propulsion Laboratory
COMMITTEE MEMBER:	Kristina Jameson, Ph.D, Propulsion Specialist at Space Systems/Loral
COMMITTEE MEMBER:	Jordi Puig-Suari, Ph.D, Professor of Aerospace Engineering

ABSTRACT

Hollow Plume Mitigation of a High-Efficiency Multistage Plasma Thruster

Scott A. McGrail

Since 2000, a relatively new electric thruster concept has been in research, development, and production at Thales Electron Devices in Germany. This High Efficiency Multistage Plasma Thruster, or HEMPT, has promising lifetime capabilities due to its plasma confinement system. However, the permanent magnet system that offers this and other benefits also creates a hollow plume, where ions are accelerated at angles rather than up the thruster centerline, causing a dip in ion current along the centerline. A laboratory model, built at JPL, was run at Cal Poly to characterize this plume shape and implement a shield to restore a conical shape to the plume. A similar solution was used on a different type of thruster, a cylindrical hall thruster, at Princeton with excellent results. A shield was designed to shunt the magnetic field outside the thruster, where the Princeton experiments have identified a radial magnetic field as the cause for this hollow plume. The thruster was run with and without the shield, taking measurements of the ion current in the plume using a linear probe drive. The shield fixed the plume shape, increasing centerline current by 48%, however it also had detrimental effects on thruster performance, causing a decrease in thrust, specific impulse, and cut the total efficiency in half. The shield design was reexamined and a new design has been suggested for future testing of the HEMPT to restore performance while still fixing the plume shape.

ACKNOWLEDGMENTS

I would just like to take a few pages to thank the many people without whom I would have never made it this far in my educational career.

First, I would like to thank Dr. Dan Goebel of JPL. Without Dan, none of this would have been possible. When I started this project, I had almost no knowledge of electric propulsion beyond the basic principles. Dan guided me through this entire project; through the work and maintenance getting the vacuum chamber and apparatus ready for testing, providing all the equipment and material needed, through the probe and shield selection and fabrication processes, the poisoning of our hollow cathode, the testing and the many, many issues that came along with it, and all the way through the analysis of the final piece of data. He not only put up with many emails a day for months, but provided excellent feedback and guidance in all of our correspondences. It is impossible for me to express how thankful I am for all of this and so much more.

An enormous thank you to my thesis advisor Dr. Kira Abercromby. Even without an expertise in EP, she has provided me with the unwavering support and motivation I needed to get through this project. She was always available whenever I had any type of issue and had a positive attitude and an incredible enthusiasm about approaching the problem and moving forward with the project. She has been a mentor to me over the past several years and I will be forever indebted to her for all she has taught me.

Thank you to the rest of my thesis committee, Dr. Tina Jameson and Dr. Puig-Suari, for their time, assistance, feedback, and guidance in this undertaking.

I would like to thank David Knapp for passing on his enthusiasm for EP testing as well as the many invaluable lessons he learned during his frustrating

time with EP testing at Cal Poly, saving me weeks of frustration because he had already been there and worked through it.

Thank you to Ryan Conversano for his help in understanding RPAs and in the construction of my grids, as well as guidance in calculations and his willingness to answer any questions I had afterwards.

Cal Poly is full of outstanding faculty and staff that is always willing to help out a student in need. A big thanks to Cody Thompson for his help in all the fabrication and machining needed for this project. Thanks to Kevin Williams for his overnight welding of all the parts I desperately needed quickly to move foward as well as the things I broke during this thesis. Thank you to Dr. Richard Savage for allowing me to borrow a helium leak detector every other week for several months during my seemingly unending attempt to achieve the base pressure necessary for EP testing in our vacuum chamber.

I would like to thank Dan Wait for allowing me to get acquainted with EP during my Senior Project, which led me down the path to this project. Dan was also very helpful in acquiring certain power supplies and the DAQ system necessary for this project.

A gigantic thank you to Sam Parker for going through this whole experience with me. Having someone in the lab during the many frustrating days attempting to get the hollow cathode or other equipment to work properly was invaluable during this process.

Thank you to Matt Stumbo for you help getting me acquainted with the lab facilities and vacuum chamber procedures and always being a phone call away when I did something wrong in the lab.

Finally, I want to extend a major thank you to my parents Mark and Wendy,

my sister Melissa, and my wonderful girlfriend Morgan for their amazing support throughout this entire process. Their positive attitude and uplifting words pushed me through the most frustrating of times during this project. Thank you all for sharing this journey with me.

TABLE OF CONTENTS

LIST OF TABLES

LIST OF FIGURES

LIST OF ACRONYMS

CEX	Charge Exchange
CHT	Cylindrical Hall Thruster
CHTpm	Cylindrical Hall Thruster with Permanent Magnets
CTFC	Coiled Tungsten Filament Cathode
DAQ	Data Acquisition System
DCFT	Diverging Cusped Field Thruster
EP	Electric Propulsion
FWHM	Full Width Half Maximum
HEMPT	High-Efficiency Multistage Plasma Thruster
HVEC	High Vacuum Equipment Corporation
JPL	Jet Propulsion Laboratory
PPM	Permanent Periodic Magnet
PPPL	Princeton Plasma Physics Laboratory
RF	Radio Frequency
RPA	Retarding Potential Analyzer
SCCM	Standard Cubic Centimeters per Minute
TED	Thales Electron Devices
TWT	Traveling Wave Tube
UHP	Ultra-High Purity

LIST OF SYMBOLS

A	open area of the thruster $[m^2]$
A_e	collection area of the probe $[m^2]$
A_{RPA}	area of the RPA probe orifice $[m^2]$
a	acceleration $[m/s^2]$
c	effective exhaust velocity $[m/s]$
e	elementary charge [1.6022x10^{-19}C]
F	force $[N]$
$f(V)$	ion voltage distribution function
g_0	gravitational constant of Earth $[9.81m/s^2]$
I	impulse $[N-s]$
I_b	beam current $[A]$
I_c	average collected ion current $[A]$
I_d	discharge current $[A]$
I_{probe}	current collected by the probe $[A]$
I_{sp}	specific impulse $[s]$
I^{++}/I^{+}	fraction of double ion current in the beam
$(j/j_0)_{Xe^+}$	CEX correction factor for singly charged ions
M	mass of an ion $[kg]$
M_f	final spacecraft mass $[kg]$
M_o	initial spacecraft mass $[kg]$
M_{Xe}	mass of a Xenon ion [131.293AMU, 2.1798x10^{-25}kg]
m	mass $[kg]$
$\dot{m}$	mass flow rate $[kg/s]$
$\dot{m}_p$	propellant mass flow rate $[kg/s]$
n_i	ion density [particles/m^2]
n_0	neutral density [particles/m^2]
P	chamber pressure [Torr]
P_k	keeper power $[W]$
$Q_{ingested}$	equivalent ingested flow rate [sccm]
$Q_{injected}$	injected flow rate [sccm]
Q_t	equivalent total flow rate [sccm]

r	radial distance from thrust centerline $[m]$
T	thrust $[N]$, neutral gas temperature $[K]$
T_g	grid transparency
t	time $[s]$
V_b	beam voltage $[V]$
V_d	discharge voltage $[V]$
V_{probe}	discriminator grid potential $[V]$
V_{RPA}	most probable ion voltage $[V]$
Z_i	ion charge state
z	axial distance from thruster to probe $[m]$
α	thrust correction factor
α_m	double ion correction factor for mass utilization efficiency
γ	total thrust correction factor
ΔV	change in spacecraft velocity $[m/s]$
η_b	beam current fraction of discharge
η_c	conductance correction factor
η_m	mass utilization efficiency
η_o	electrical efficiency
η_T	total thruster efficiency
η_v	beam voltage fraction of discharge
θ	beam divergence half-angle
σ_1	effective cross sectional area of singly charged ion $[\mathring{A}^2]$
ϕ_p	plasma potential $[V]$

1. INTRODUCTION

1.1 MOTIVATION

As the aerospace industry continues to move forward and advance the technologies used for spacecraft propulsion, electric propulsion has become a promising choice for spacecraft developers. These electric propulsion systems offer considerable propellant mass savings over traditional rocket engines and have become increasingly reliable and desired for spacecraft. New designs and improvements are essential to ensure that EP remains a prime choice in the spacecraft community. This thesis provides the opportunity to dive headfirst into the world of electric propulsion development and testing, a world that I would like to continue to be a part of as I move out of academia and into the aerospace industry.

1.2 THESIS STATEMENT

The purpose of this thesis is to mitigate a "hollow plume" on a High-Efficiency Multistage Plasma thruster through the implementation of a magnetic shield. This thruster has a strong, largely axial magnetic field outside the ceramic channel that accelerates ions at large divergence angles rather than along the thruster centerline, causing a dip in ion current at the centerline. The shield will attempt to shunt this region of the magnetic field and restore a conical shape to the plume. Through the use of a Retarding Potential Analyzer, the ion plume shape

will be characterized, along with the thruster performance, before and after the implementation of this shield.

2. ELECTRIC PROPULSION BACKGROUND

2.1 ROCKET PROPULSION BASICS

One of the essential systems on a spacecraft is the propulsion system, which is utilized to move the vehicle, release excess momentum, or orient the spacecraft. Energy is required to get a spacecraft into space, move from one orbit to another, maneuver to certain attitudes, or counteract the perturbations which try to remove a spacecraft from its desired orbit. The propulsion system is most often utilized to deliver this energy. Propulsion systems convert electrical or chemical energy into kinetic energy in the form of a velocity change.[9, 22] Whether chemical or electrical energy is used, the propulsion system ejects mass from the spacecraft, often at high exhaust velocities, and relies on the principle of conservation of momentum to move the spacecraft. The ejection of mass at high velocities causes a reaction that pushes on the spacecraft structure providing that change in velocity, or ΔV. This force is called thrust, T, and is caused by the ejection of propellant. The Rocket Equation is a standard formula used to describe the spacecraft motion, and follows Newtons second law of force equals mass times acceleration in the form [9, 22]

$$T = m\left(\frac{dv}{dt}\right) \tag{2.1}$$

where T is the thrust force in Newtons, m is the spacecraft mass, and dv/dt is the change in velocity with respect to time in meters per second squared. The

total impulse of the spacecraft in Newton-seconds can be found by integrating the thrust over the time spent thrusting,[22]

$$I = \int F dt. \tag{2.2}$$

The specific impulse, which is used as a measure of rocket performance, is the total impulse divided by the unit weight of the propellant,[22] as shown in the equation

$$I_{sp} = \frac{T}{\dot{m} \cdot g_0} \tag{2.3}$$

where $\dot{m}$ is the constant propellant mass flow rate in kilograms per second, T is the constant thrust in Newtons, and g_0 is the acceleration due to gravity at 9.81 meters per second squared. Specific Impulse can also be expressed in terms of the effective exhaust velocity,[9]

$$I_{sp} = \frac{c}{g_0} \tag{2.4}$$

where c is the effective exhaust velocity in meters per second. The change in velocity of the spacecraft can be found in terms of the propellant expelled during a thrusting event, or burn, through the equation

$$\Delta V = I_{sp} \cdot g_0 \cdot ln\left(\frac{M_0}{M_f}\right) \tag{2.5}$$

where M_0 is the total spacecraft mass before the burn and M_f is the total spacecraft mass after the burn.

Traditional rocket engines use a chemical reaction to create a rapidly expanding gas that is accelerated out a nozzle in order to produce the thrust force. Electric propulsion (EP) uses electric and magnetic fields to accelerate energetic ions out of the thruster. EP will be discussed further in the following section.

2.2 ELECTRIC PROPULSION

While chemical propulsion systems usually have exhaust velocities in the range of $3 - 4$ km/s, electric propulsion systems can reach up to 10^3 km/s.[9] Referring back to Equation 2.4, the specific impulse of a thruster is directly proportional to its effective exhaust velocity. Consequently, electric thrusters have very large specific impulses compared to chemical thrusters.

Two of the most common types of EP thrusters are ion thrusters and Hall thrusters. Ion thrusters use biased grids at the thruster exit to accelerate the ionized propellant out of the chamber, while Hall thrusters use a radial magnetic field in the channel to trap electrons and create an axial electric field that accelerates the ions.[9] Images of a BPT-4000 Hall thruster developed at Aerojet and JPL's NEXIS ion thruster during operation are shown in Figure 2.1.[2]

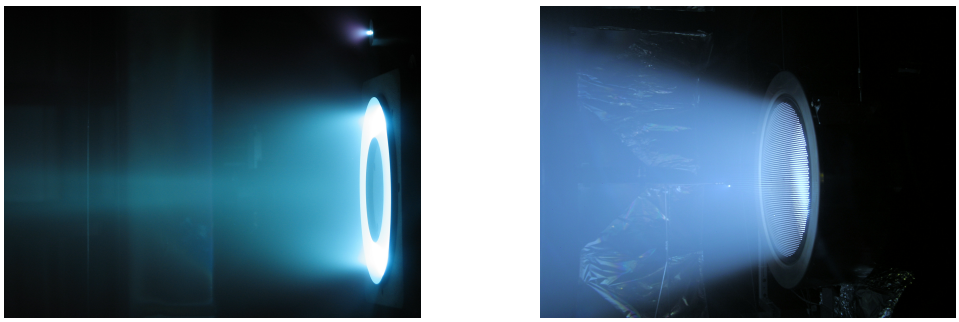

(a) (b)

Figure 2.1: (a) An Aerojet BPT-4000 Hall thruster[2] (b) A NEXIS ion thruster developed at JPL[2]

The NEXIS ion thruster has the capability of operating at 20kW and achieve an Isp of 7000 seconds, while the Aerojet BPT-4000 can operated in the 1-5kW range and achieve an Isp of 2000s.[9] Ion thrusters typically have higher specific impulses than Hall thrusters, however Hall thrusters are usually simpler devices with less complex power systems.[9]

An ion thruster usually has a discharge chamber into which an electron source initiates a plasma. An anode is biased to a high positive voltage and the ions in the chamber moves toward a series of biased grids near the exit of the thruster. These grids or screens are used to keep electrons in the chamber while accelerating out the ions to form the beam and create thrust.[9] The accelerated ions in the beam are then neutralized through the use of a hollow cathode or other electron source. This principle is graphically represented in Figure 2.2

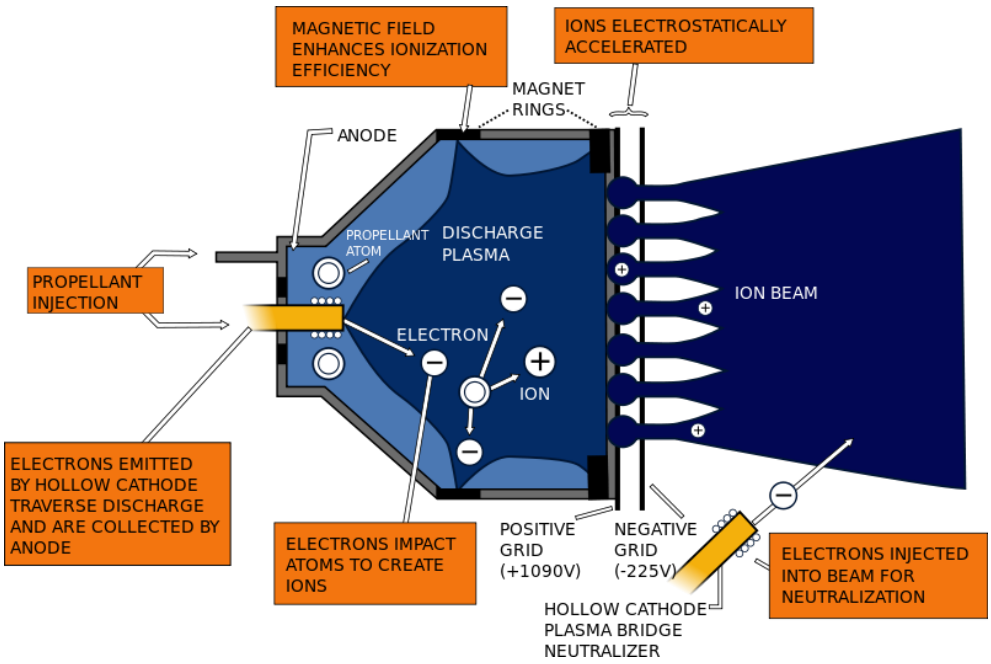

Figure 2.2: The operational principle of a ion thruster[3]

Hall thrusters typically consist of a cylindrical or annular channel into which a neutral propellant is injected. Most commonly, electromagnets create a largely radial magnetic field in the channel. A electron source creates electrons that are drawn toward the anode at the base of the channel, however the radial magnetic field catches these electrons in a ExB drift and prevents electrons from reaching the upstream anode. The trapped electrons rotate around the channel creating the Hall current for which the thruster is named. These electrons also ionize

the neutral propellant in the channel. Ions are accelerated out of the channel due to the electric field between the anode and cathode potential outside the thruster.[9] These ions are then neutralized by more electrons from the cathode electron source, like in the ion thruster. These principles are shown in Figure 2.3.

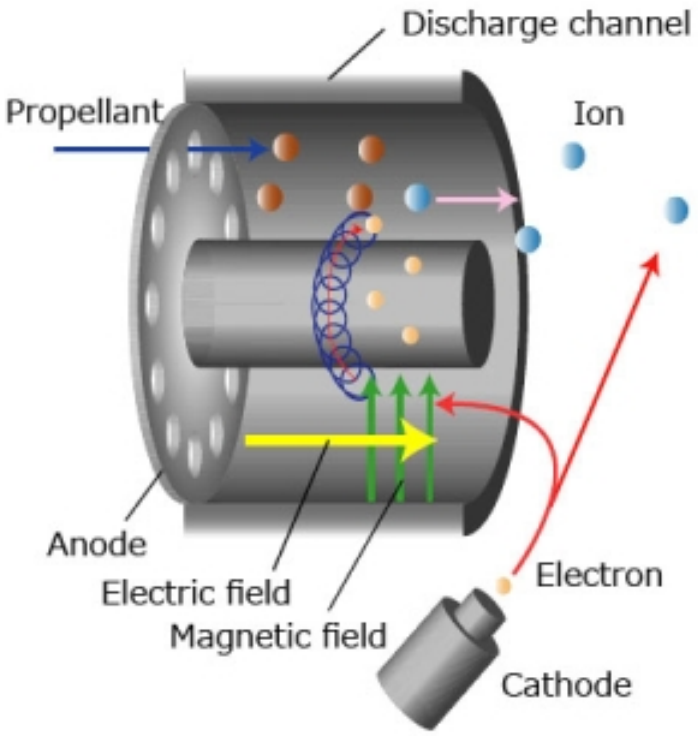

Figure 2.3: The operational principle of a hall thruster[1]

Both ion and Hall flight thrusters typically use hollow cathode neutralizers in their standard configurations. Hollow cathode electron sources were developed to solve the problems posed by coiled tungsten filament cathodes (CTFCs) used in early ion thrusters, which include low efficiency due to heating and a very limited lifespan, among others.[9, 14] A hollow cathode consists of a hollow tube with an orifice at the exit. An insert is placed in the tube, which acts as the electron emitter. A heater is also wrapped around the cathode tube to facilitate electron emission of the insert by raising the temperature to an emissive temperature.[9] A keeper electrode typically encloses the rest of the cathode and facilitates the

turn-on of the cathode as well as maintain cathode temperature during operation and protect the remainder of the components from ion bombardment which can reduce the life of the unit.[9] These components are represented in Figure 2.4.

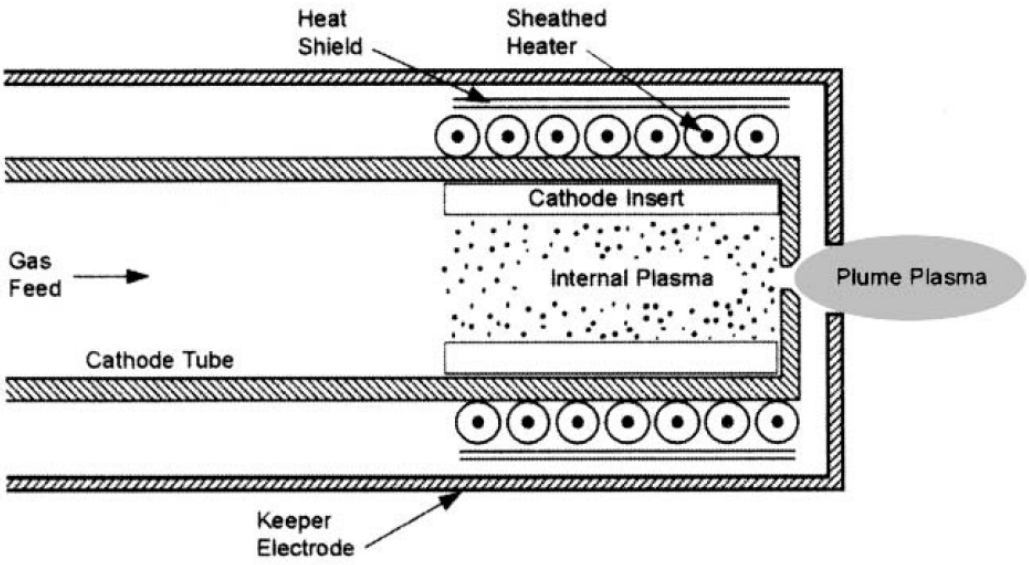

Figure 2.4: The components that make up a hollow cathode electron source[9]

While ion and Hall thrusters are the most well-known of electric propulsion types, research and development of new electric thrusters is always underway. The following section will detail a relatively new thruster concept that is used and tested in this thesis.

3. THE HIGH-EFFICIENCY MULTISTAGE PLASMA THRUSTER

3.1 BACKGROUND

The concept for the High-Efficiency Multistage Plasma Thruster (HEMPT) was developed at Thales Electron Devices (TED) in the mid-1990s and refined in the early 2000s. TED does extensive work with traveling wave tubes (TWTs), used to amplify RF signals for spacecraft communications. The TWTs use a controlled electron beam to amplify these signals from a few milliwatts to about 100 Watts. Generated in an electron gun, the electron beam is focused to a specific diameter using a permanent period magnet (PPM) system. This PPM system creases magnetic forces that counteract radial space charge forces in the beam.[18, 16] The TWT and PPM systems are graphically represented in Figure 3.1.

In 1996, TED decided to take their PPM system technology and apply it to electric propulsion. They believed that the magnetic field configuration would keep the plasma off the walls of the discharge channel. The magnetic field topography would allow for a multi-stage plasma chamber where each magnetic cell region would decrease in potential towards the thruster exit, reducing kinetic energy losses of channel electrons to the anode. The system would also include a fast primary electron beam through the use of an electron gun in order to initiate propellant ionization in the chamber and neutralize ions at the exit. After testing this new system, it was realized that this design was not useful or feasi-

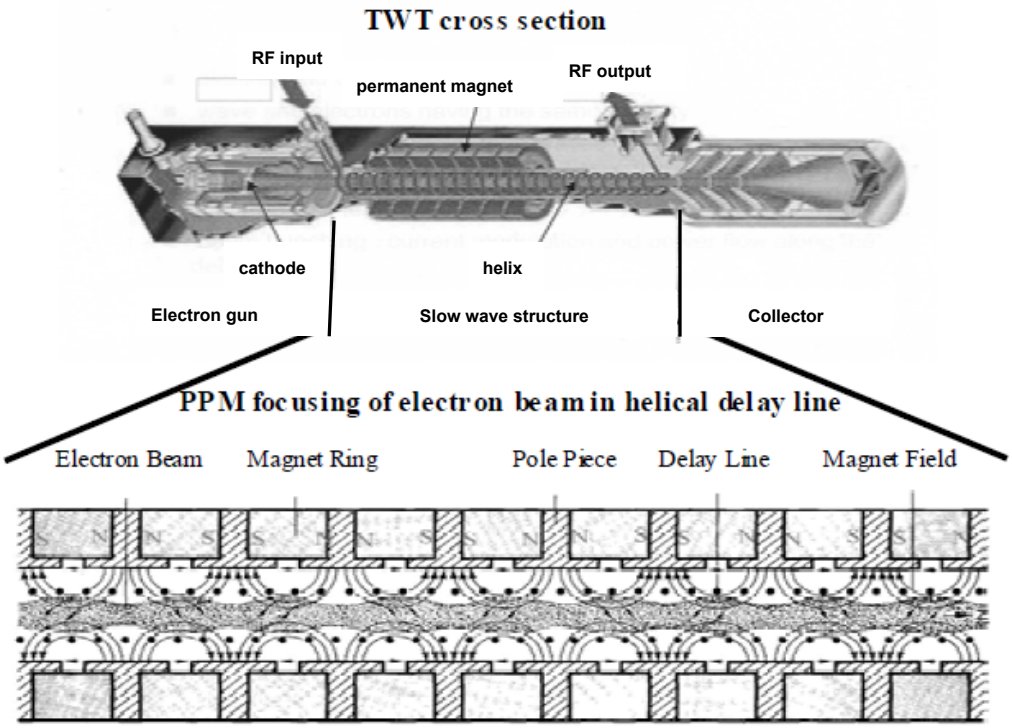

Figure 3.1: TWT cross section and PPM operational diagram[18]

ble. Extensive erosion was observed due to the electron gun, cathode emission was strongly poisoned, few electrons made it downstream of the thruster, and segment voltages self-adjusted due to low impedance.[18, 17, 16]

In 2001, the following changes were made that modified the original design:[18]

- The electron gun was removed and replaced with a standard neutralizer (hollow cathode) at the thruster exit
- The neutral propellant was injected at the anode rather than the electron gun
- A thin tube was inserted to isolate the segmented electrodes from the plasma in the discharge channel
- The permanent magnet fixture was improved

- Discharge chamber diameter adapted to better work with the magnetic field configuration.

These modifications, in conjunction with plasma simulations and hardware improvements led to overall thruster progress and a glimpse of the concept's potential, concluding with the final configuration of the HEMPT detailed in the following section.[18]

3.2 CONFIGURATION

In the basic HEMPT design, neutral propellant is injected into the discharge chamber at the anode. The dielectric discharge chamber is made of an insulating ceramic tube, separating the plasma in the channel from the PPM system. The PPM system alternates the polarity of the magnet rings along the length of the discharge channel. The design in this thesis has three rings of magnets, creating three magnetic cusps separating the "stages" of the plasma. Figure 3.2 shows some of the operating principles internal to the HEMPT configuration.[15, 17, 18, 16]

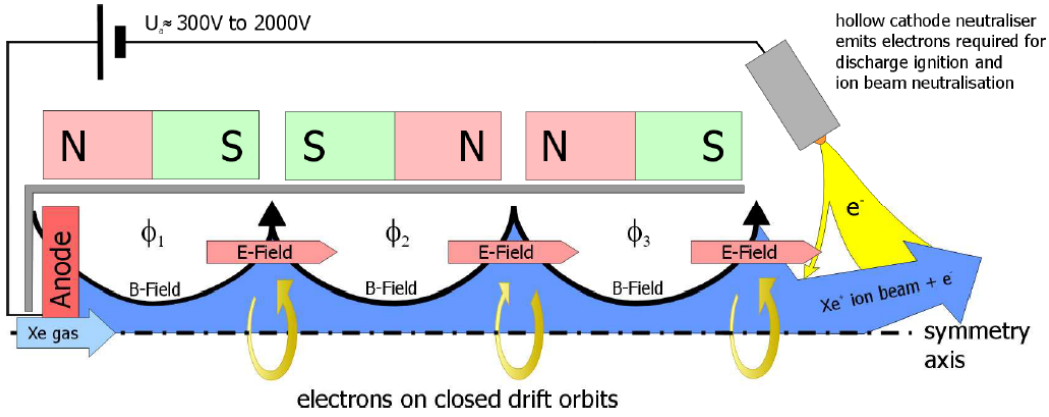

Figure 3.2: The internal physics of the HEMP thruster concept[10, 16]

The hollow cathode plasma source placed outside the thruster supplies the electrons that both ionize the neutral propellant in the thruster and neutralizes

the ions in the beam. Electrons are attracted to the high discharge potential of the anode and therefore attempt to travel upstream toward the anode. The strong radial magnetic field regions at each magnetic cusp catch electrons on a ExB drift orbit. Each magnetic "cell" increases in potential moving toward the anode, making it harder for channel electrons move upstream to the anode. Plasma simulations and measurements during HEMPT development show a steep potential gradient between the first and second cells, inducing most of the ion acceleration in this region, while the second and third cells contribute to discharge stability and formation of the ion beam.[15, 17, 18]

The PPM system confines most electrons to the magnetic cells,which reduces electron contact of the channel walls.[15, 17, 16] High-energy particle collisions with the wall include a transfer of energy, removing some from the thrust output and reducing efficiency. Collisions like this also lead to erosion of the walls, as seen in Hall thrusters. In-depth testing has shown that HEMP thrusters are free from the wall erosion, which leads to longer life and increased efficiency.[15, 16]

3.3 LABORATORY HEMPT AND HOLLOW CATHODE

The HEMPT used for the testing in this thesis is a laboratory model built at JPL for research purposes. It was donated for use in this thesis. The anode and thruster body are made of stainless steel, the channel is a ceramic tube, the magnets are Samarium Cobalt magnets placed 10 to a ring on iron discs that make up the magnetic poles and separate the alternating rings. The magnets are very strong and sometimes pop out of their respective rings. To prevent this, a high temperature wire was wrapped and tightened around each ring to keep the magnets in place during testing.

The hollow cathode is also a laboratory model built at JPL and donated for electric propulsion projects at Cal Poly. The cathode has a 1/4 inch diameter insert. The HEMPT and hollow cathode can be seen in Figure 3.3.

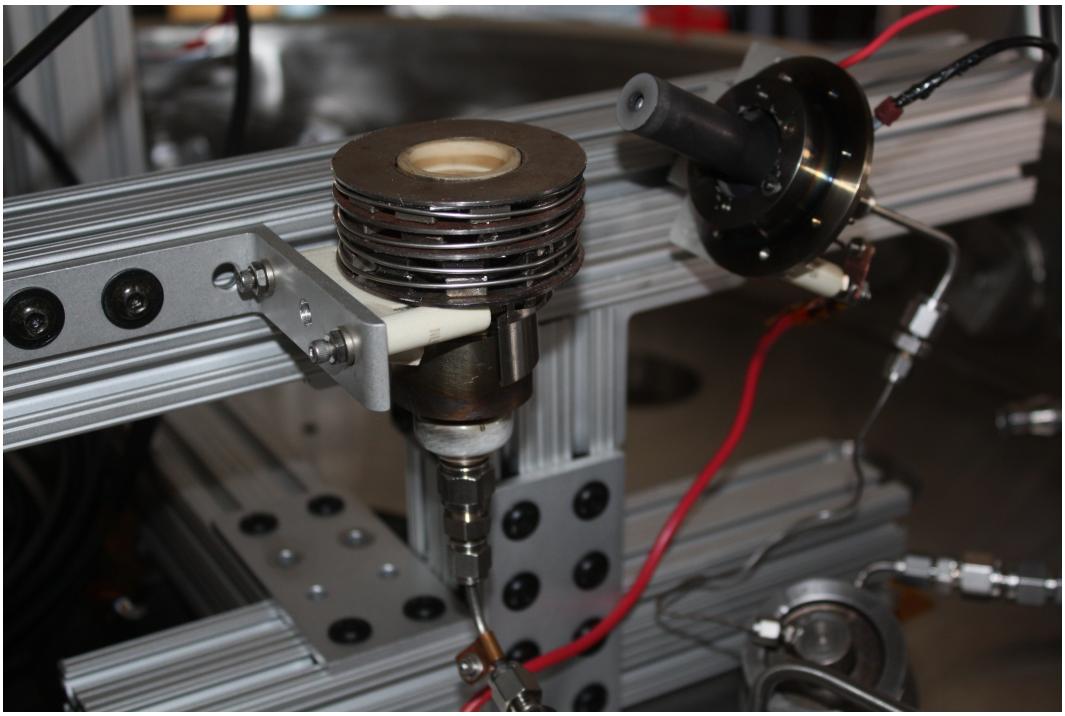

Figure 3.3: The HEMPT and hollow cathode set up in the vacuum chamber

3.4 HOLLOW PLUME & PROPOSED SOLUTION

While the HEMPT's PPM system provides several benefits, there is also a major drawback. The magnet configuration locates one of the cusps next to the thruster exit. While this cusp aids in impeding electron travel to the anode and in acceleration of ions out of the thruster, it also causes a strong magnetic field outside the thruster channel that wraps around to the face of the first magnet ring, clearly visible in Figure 3.4a. This strong magnetic field has a large impact on the shape of the plasma plume. It has been observed that the plume has a

"hollow" shape, where there is more ion current offset from the centerline than on the centerline itself. This phenomenon has adverse effects on thrust generation of the HEMPT. The hollow plume can be seen in Figure 3.4.

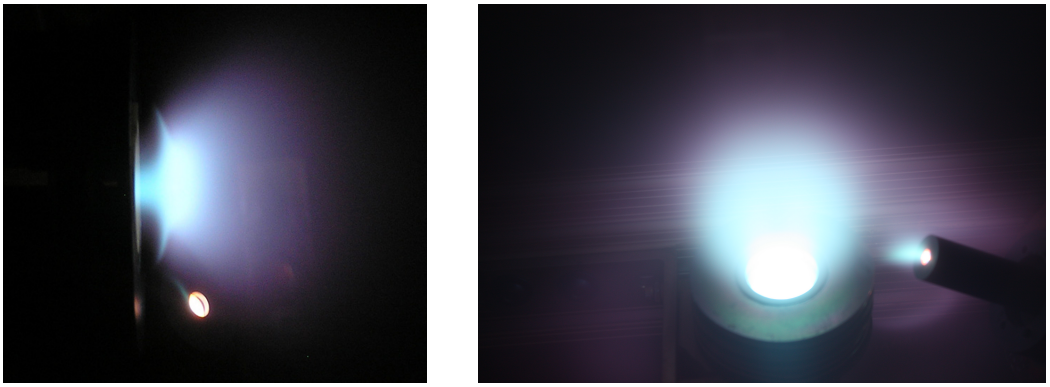

(a) (b)

Figure 3.4: (a) A side view of the HEMPT during operation at JPL with strong magnetic field and hollow plume visible [Photo credit: JPL] (b) A view of the HEMPT during operation at Cal Poly

Other plasma thrusters, such as cylindrical Hall-thrusters (CHT's) and diverging cusped field thrusters (DCFT's) have a similar issue.[5, 20, 19] The DCF magnet design was inspired by the PPM system used in the HEMPT, therefore it experiences some of the same types of issues.[5] The CHT with permanent magnets had a cusped magnetic field near the exit of the ceramic channel, similar to that seen in the HEMPT.[20, 7] In-depth investigation has been done at the Princeton Plasma Physics Laboratory (PPPL) into the effect of this outer magnetic field on plume shape for the CHT. These investigations have shown that the strong magnetic field outside the thruster is actually a significant area of ion acceleration; up to 50% of ion acceleration actually takes place outside the thruster.[19] Since there is a strong radial magnetic field in this region, the ions are accelerated off at angles rather than straight up the centerline of the thruster.[20, 19, 7]

In order to mitigate this hollow plume issue, a magnetic shield will be im-

plemented on the HEMPT with the goal of reducing the outer magnetic field and restoring a conical shape to the plume. The team at PPPL implemented a low-carbon steel shield onto their CHT with permanent magnets (CHTpm) and observed excellent results.[20, 19] Results of the shielded CHTpm experiments showed plume change from the hollow shape into a typical conical type with maximum ion current along the centerline, along with a narrowing of the plume.[19, 7] The shield configuration and experimental results of the CHT testing is in Figure 3.5.

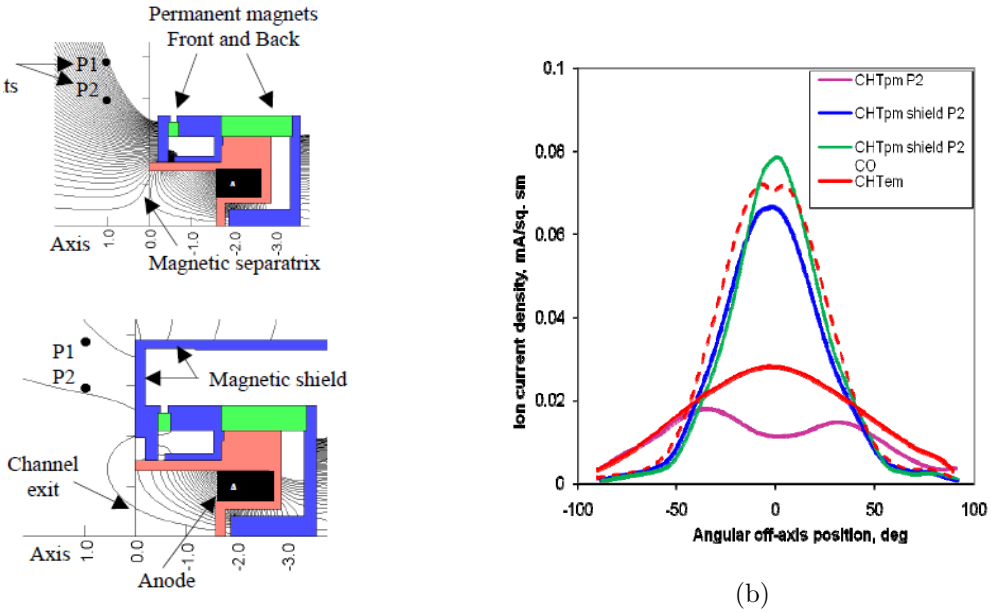

Figure 3.5: (a) The magnetic field simulation and shield configuration for the PPPL CHTpm with shield (b) Results of the CHTpm with shield testing, shielded plots in blue and green [19]

The CHTpm plume has ion current peaks out around 30 degrees from the thruster centerline. Based purely on the visible plume from Figure 3.4a, the ion current peaks for the HEMPT are expected to be located a bit closer to the centerline, perhaps at an offset around 15 to 20 degrees.

Due to the success of the magnetic shield on the CHTpm, a magnetic shield will be designed and fabricated out of iron for implementation on the HEMPT in the hopes of achieving similar positive results, which include a narrowing of the plume divergence and an increased centerline ion current. The design of this shield will be detailed in the following section.

4. 2D STATIC MODELING

In order to provide a basis of proof for the proposed solution of adding an iron shield to the HEMPT, the thruster was simulated in an electromagnetic field modeling program called MagNet v7 made by Infolytica. Since the free trial of the MagNet software was used, the program was limited to a two-dimension magnetostatic solver. It should be noted that this modeling of the HEMPT's magnetic field is used only as a tool for design. No validation of these models was performed or required within the scope of this thesis.

4.1 CONSTRAINTS

The design of the shield was constrained by several factors. The cast-iron material used to manufacture the shield was provided with the HEMPT by Dr. Goebel at the beginning of the thesis. Since the material was provided, no investigation into other shield material was performed. However, due to the ferromagnetic properties of iron, the provided material was best-suited for the task of shunting the magnetic field anyway. The material was provided in a cylinder with a three inch diameter and a three inch height. This constrained the outer diameter of the shield to a maximum of three inches.

The length of the shield was limited by the thruster's configuration on the stand. In order to ensure the shield did not contact the aluminum frame of the

stand, the length of the shield could not exceed 0.8" from the thruster exit.

4.2 MODELING

Only components essential to the actual magnetic field structure were modeled in MagNet. These components included the the stainless steel anode and thruster body walls, iron pole rings, and permanent Samarium Cobalt magnets. The ceramic channel that makes up the chamber was not included due to its negligible effect on the magnetic field. Before any shields were added, the original thruster was modeled in order to provide comparison of the magnetic field strength at strategic places with and without a shield.

The HEMPT is assumed to have axial symmetry about the thruster centerline. Due to this assumption, only half of the thruster's cross section was created in the program. Each object was created in two dimensions and then extended one inch backward in the third dimension. Only a single "slice" of the 3D object was able to be electromagnetically modeled, therefore a 2D solution was provided by the program. The initial model of the thruster is shown in Figure 4.1.

The material for each object was selected from a library of pre-programmed materials in MagNet. The magnets were made of "Samarium Cobalt", the iron pole pieces and shields from "Remko: Soft pure iron", and the stainless steel parts from "S416: 416 Grade Stainless Steel." While some of these material selections are not exact, they provide a close estimate of the material properties of the actual thruster components for the model.

MagNet automatically creates and refines the mesh during solving based on certain input parameters from the user. A Newton-Raphson method was used in the solver followed by a h-adaption that automatically selected the worst 25% of

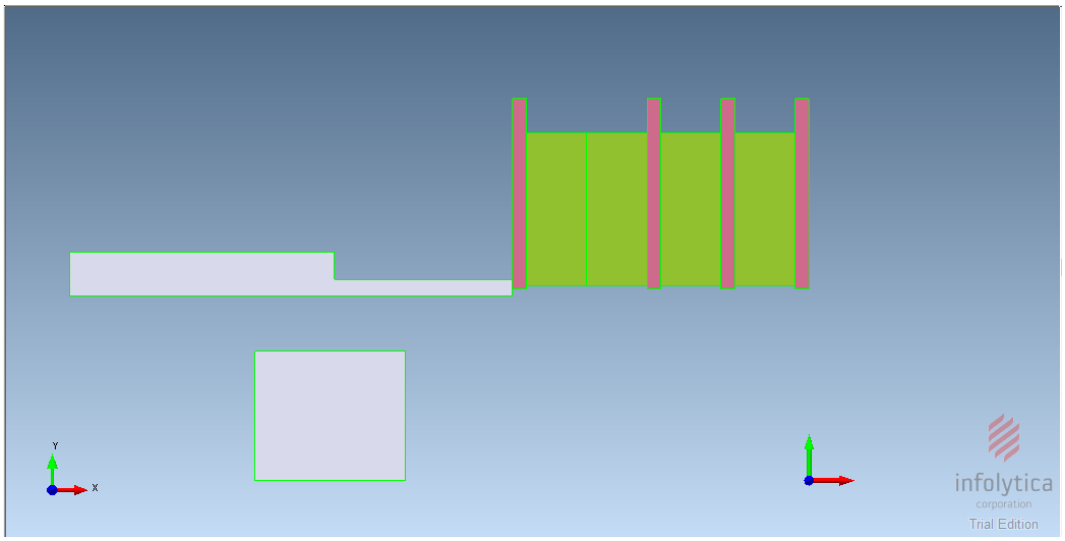

Figure 4.1: The MagNet model of the HEMPT with stainless steel components in gray, magnets in green, and iron components in pink

the elements and created new elements with half the dimension of the original elements until a tolerance of 0.1% was reached. This refined mesh created by the program provides high resolution in areas where a large gradient is present in the solution. The solution mesh is acceptable for use in this thesis since the results are used in a design tool capacity, however a higher resolution mesh or solution were never created and therefore no comment can be made on the benefits of using such a mesh for the solution. An initial mesh of the model alongside the final solution mesh created through the adaptation process are shown in Figure 4.2.

The solution generated by MagNet can be shown in numerous ways. The most useful visible solution image for the purposes of this thesis includes a shaded plot of the magnetic field strength overlaid by a contour plot of the magnetic flux lines. In order to provide consistency between solutions, all solution images shown in this section have the same scale for both the shaded and contour plots. The solution for the original HEMPT configuration is shown in Figure 4.3.

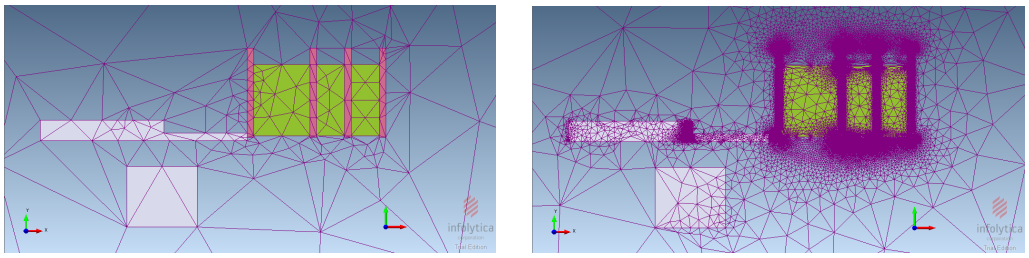

(a) (b)

Figure 4.2: (a) The initial mesh automatically generated by MagNet (b) The final solution mesh with refined elements

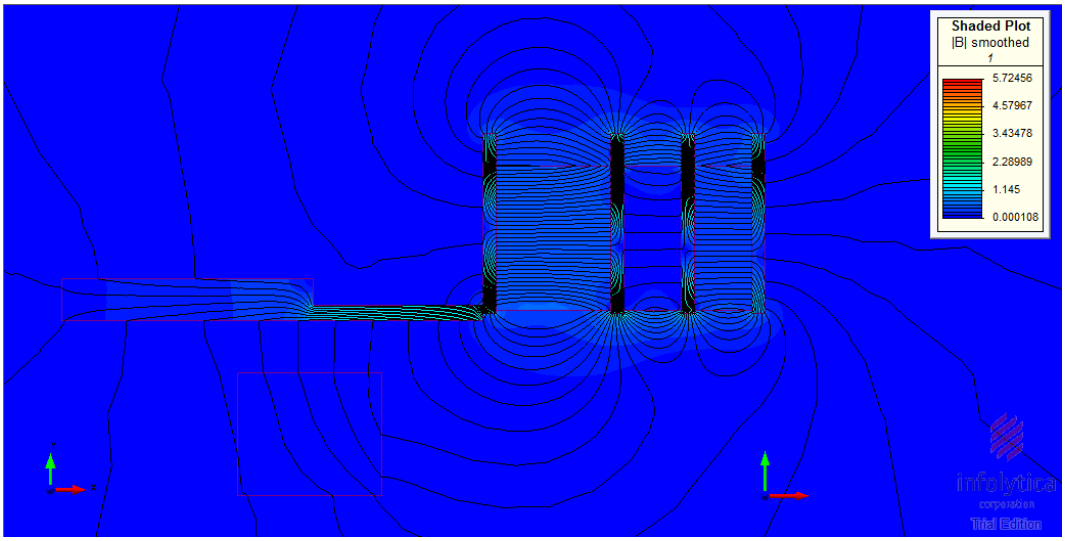

Figure 4.3: The electromagnetic solution for the original HEMPT configuration

4.3 SHIELD DESIGN

Six shields were initially designed and modeled in MagNet in order to examine the effect of parameters such as a chamfered opening, face thickness, wall thickness, wall location, and wall length on the magnetic field. After the implementation of each shield into the model, the radial and axial magnetic fields were examined at certain locations within and outside the HEMPT with an emphasis on reducing the overall magnetic field strength outside the thruster channel, but especially in

the radial direction. The configuration of the thruster is the same in all models, the axial magnetic field direction is right while the radial magnetic field direction is up. While the effect of varying certain shield parameters was observed, the goal of the modeling does not include finding an "optimum" shield. These variations aided in the design but no formal optimization was used.

Shield 1 is the basic starting shield, with uniform wall and face thicknesses of 0.2" and the inside diameter of the shield opening at the thruster exit is even with the outside diameter of the ceramic channel. The opening diameter of the shield will remain constant throughout the selection process. Shield 2 has the same configuration as Shield 1, however a 45 degree chamfer is added to the inner diameter of the shield opening. Shield 3 examines whether a thinner face of 0.1" provides any benefit over the nominal face thickness. Shield 4 leaves the face thickness at 0.2" and changes the wall thickness to 0.1", as well as places the wall further away from the magnets. Shield 5 is similar to Shield 4 except the wall is moved 0.1" closer to the thruster. Finally, Shield 6 examines whether a shorter shield wall at 0.5" length rather than the nominal 0.8" provides any benefits to the HEMPT magnetic field. These six shields are presented in Figure 4.4.

4.3.1 MODELING RESULTS

As each shield is examined in numerical order from 1 to 6, it will be compared to the original HEMPT as well as the previous "best" shield. The "best" shield will have had the most significant reduction of magnetic field strength outside the thruster. Three line plots of magnetic field strength in the axial (z) and radial (r) directions will be used to determine the reduction. These line plots are located along the thruster centerline, along the inner wall of the discharge channel, and a half-inch outside the thruster from the centerline to a radius of 5 cm.

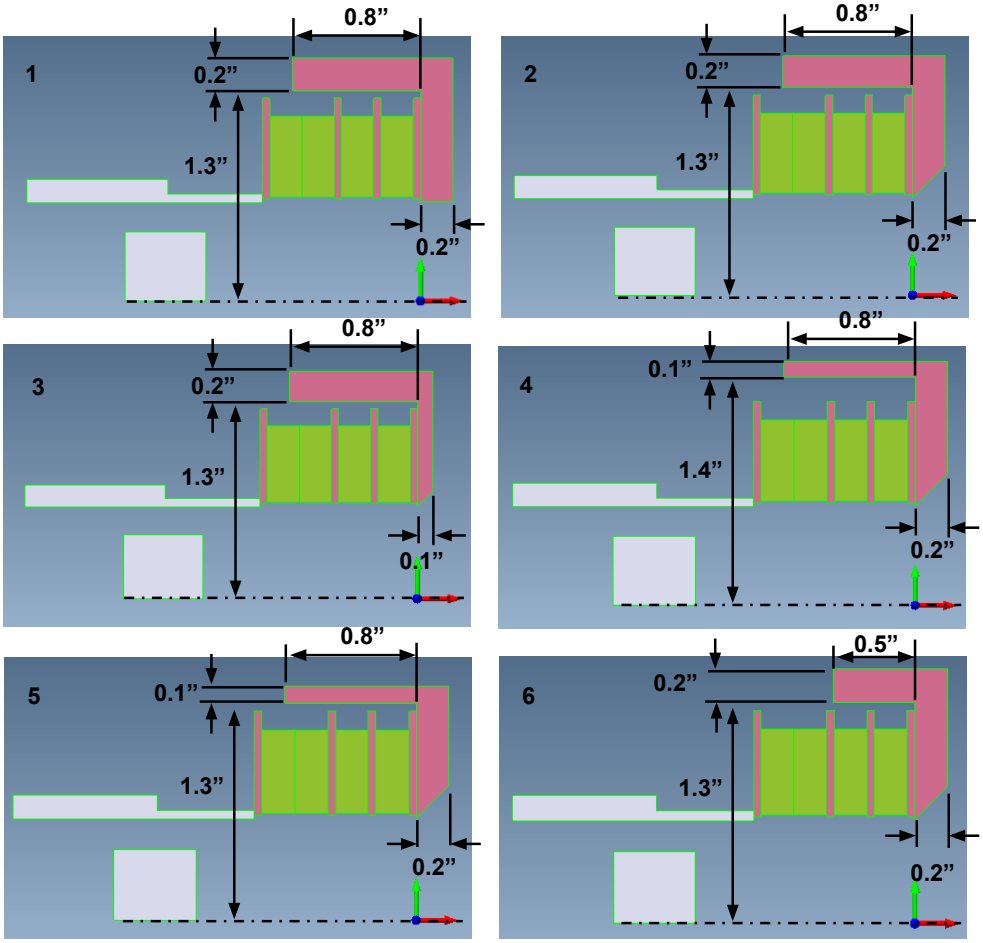

Figure 4.4: The six shields that were modeled and examined in MagNet

4.3.1.1 SHIELDS 1 AND 2

The modeling results of Shields 1 and 2 are presented together and compared to the original HEMPT magnetic field results. The main difference between these two shields is a chamfered opening. The magnetic field line plots are shown in Figure 4.5.

Examination of Figure 4.5 shows that Shield 2 provides maximum reduction of the radial magnetic field outside the thruster exit when compared to Shield

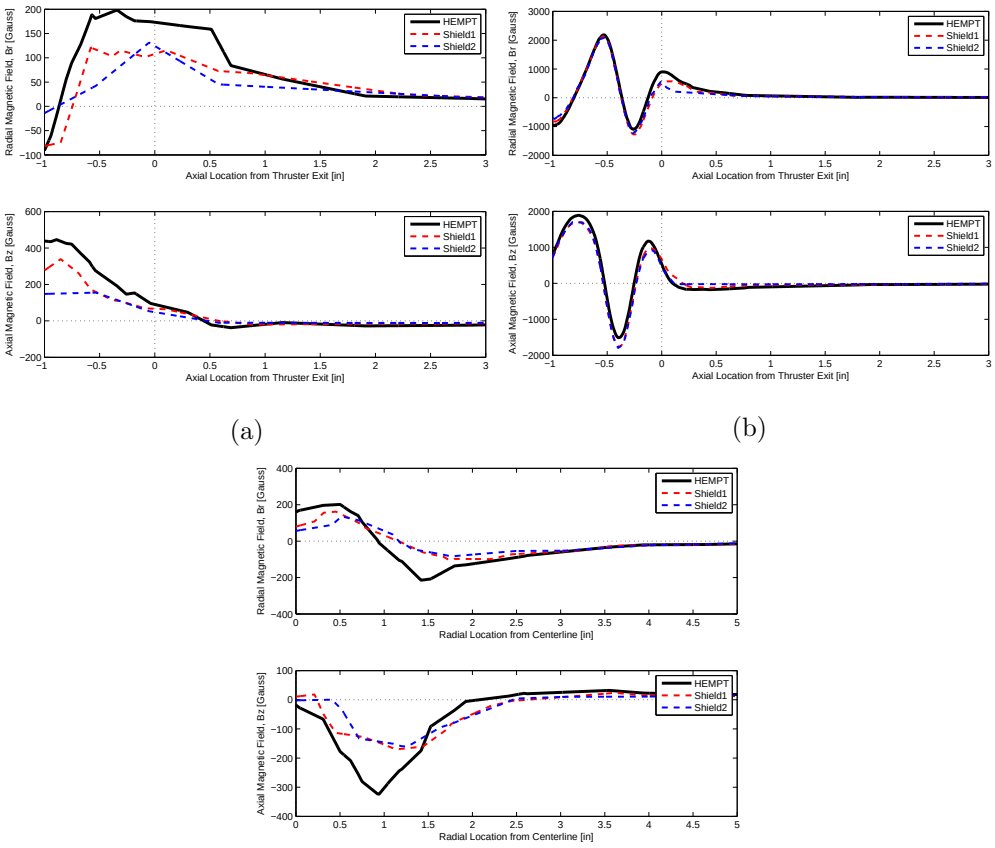

Figure 4.5: Shields 1 and 2 magnetic fields (a) along the thruster centerline (b) along the thruster channel wall (c) 1/2" outside thruster

1. Since the only difference between these two designs is the 45 degree chamfer at the opening, this feature seems to have a positive and significant effect on the magnetic field and therefore all subsequent shields will include this chamfer. This desirable effect allows the shield selection to move forward using Shield 2 as the current "best" shield design.

4.3.1.2 SHIELD 3

Now that it has been established that the general shape of the shield reduces the magnetic field outside the thruster, small changes will be made to the shield

parameters. Shield 3 cuts the shield face thickness in half while leaving all other dimensions unchanged. The magnetic field line plots are shown in Figure 4.6.

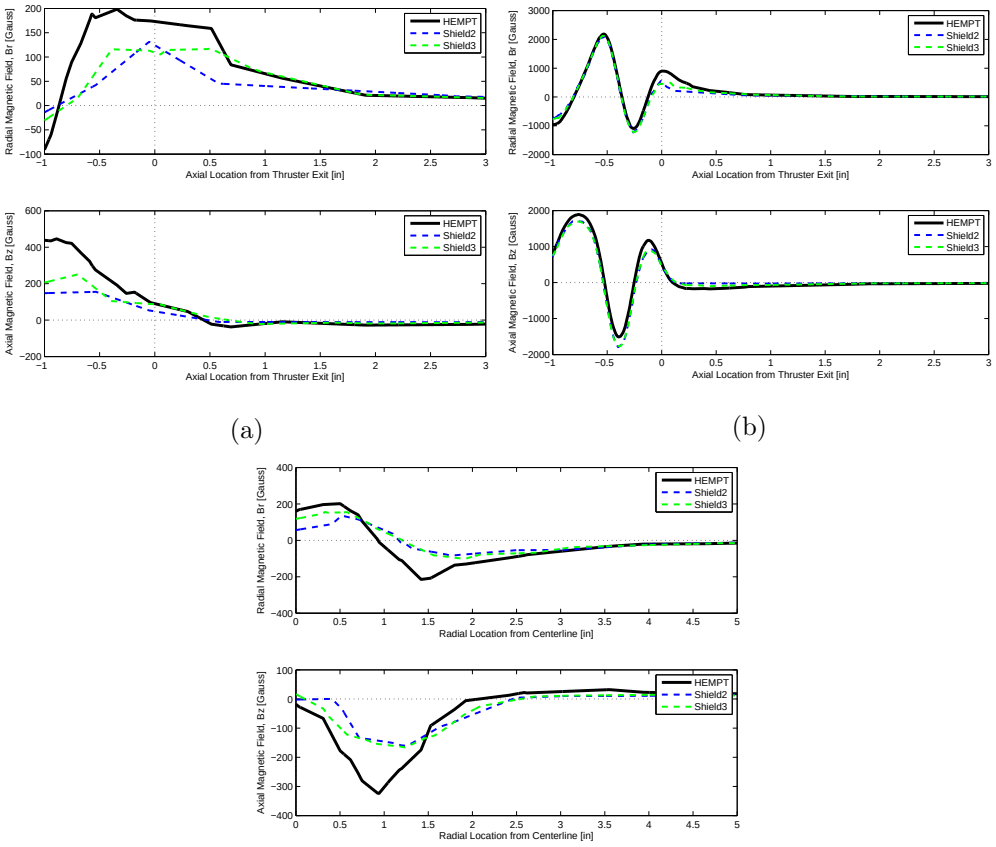

Figure 4.6: Shields 2 and 3 magnetic fields (a) along the thruster centerline (b) along the thruster channel wall (c) 1/2" outside thruster

Shield 3 provides no benefit to the radial magnetic field outside the thruster over Shield 2. In fact, most of the radial magnetic field is increased within the first inch from the thruster exit face. Using this fact, Shield 2 remains the "best" shield choice moving forward through the rest of the shield examinations.

4.3.1.3 SHIELDS 4 AND 5

Changing the face thickness does not provide any beneficial reductions in the field outside the thruster. Shields 4 and 5 aim to see if changing the wall thickness or location relative to the magnets positively changes the field. Shields 4 and 5 walls are half the thickness of the nominal wall. Shield 4 is radially 0.1" further from the magnets than Shield 5. The magnetic field line plots are shown in Figure 4.7.

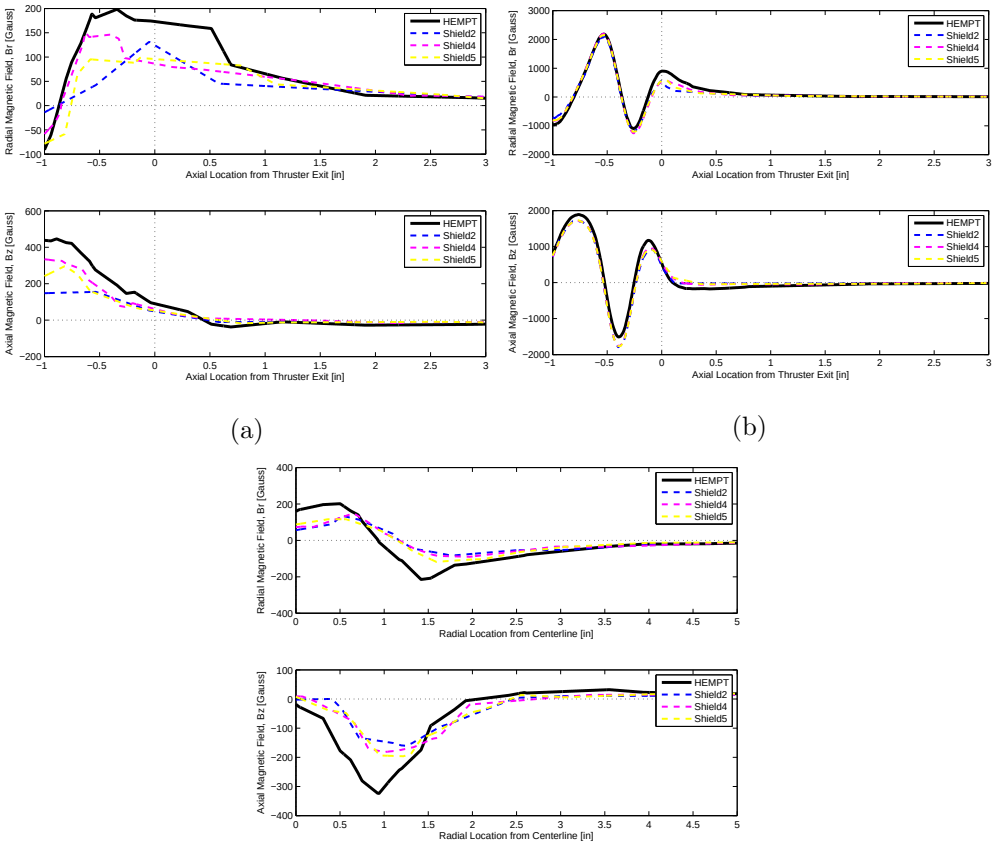

Figure 4.7: Shields 4 and 5 magnetic fields (a) along the thruster centerline (b) along the thruster channel wall (c) 1/2" outside thruster

Both Shield 4 and Shield 5 show some reduction of the radial magnetic field along the thruster centerline within the first 1/2" outside the thruster, however after that Shield 2 takes over. Also, along the wall of the channel and at a

distance 1/2" outside the thruster, Shield 2 still provides the maximum radial reduction.

4.3.1.4 SHIELD 6

The final shield parameter change that was examined was the length of the wall. The nominal wall length was 0.8" from the thruster exit plane. This was cut down to 0.5" from the exit. These results are presented in Figure 4.8.

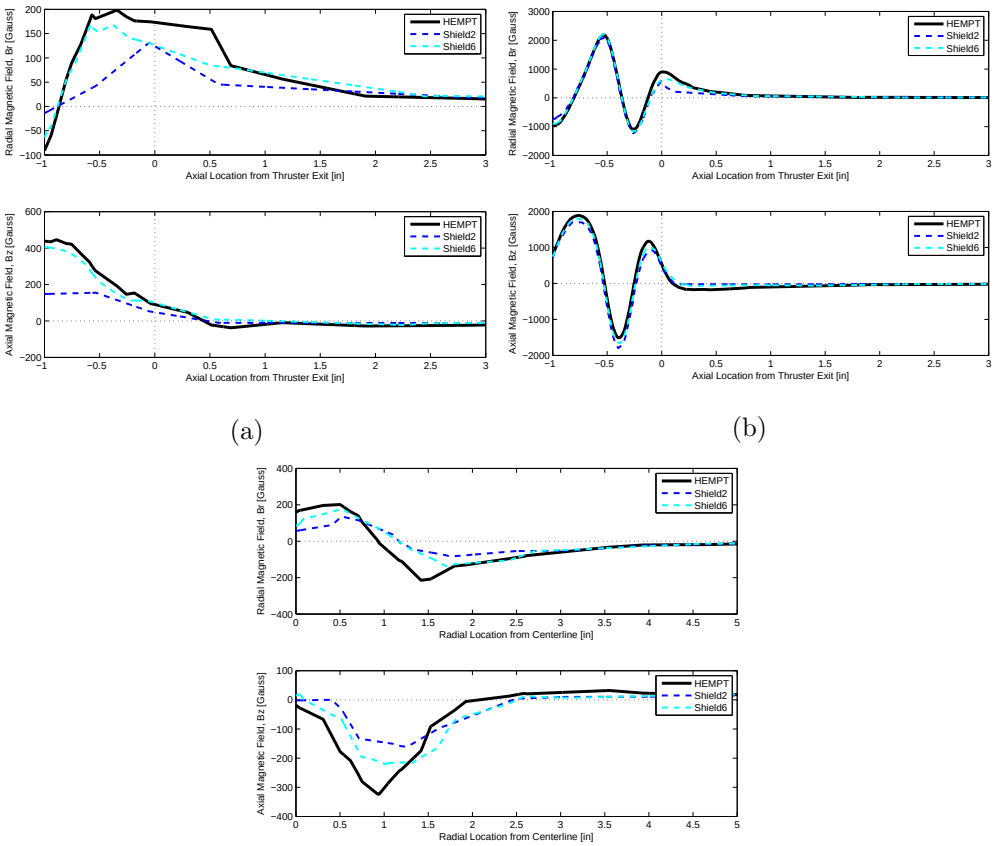

Figure 4.8: Shield 6 magnetic fields (a) along the thruster centerline (b) along the thruster channel wall (c) 1/2" outside thruster

A quick examination of the magnetic field line plots is enough to show that shortening the length of the walls does not provide any benefit for the outer

magnetic field over Shield 2.

4.3.1.5 SHIELD MODELING CONCLUSIONS

Based on the above models and comparisons of the 6 original shields examined, it can be concluded that Shield 2 provides the maximum benefit of B-field reduction outside the thruster. The final shield design has a uniform 0.2" thickness of the shield face and walls, and includes a 45 degree chamfer on the shield opening. The MagNet solution plot of the magnetic field strength and flux lines of original HEMPT is shown again in Figure 4.9 while the chosen shield, Shield 2 is presented in Figure 4.10.

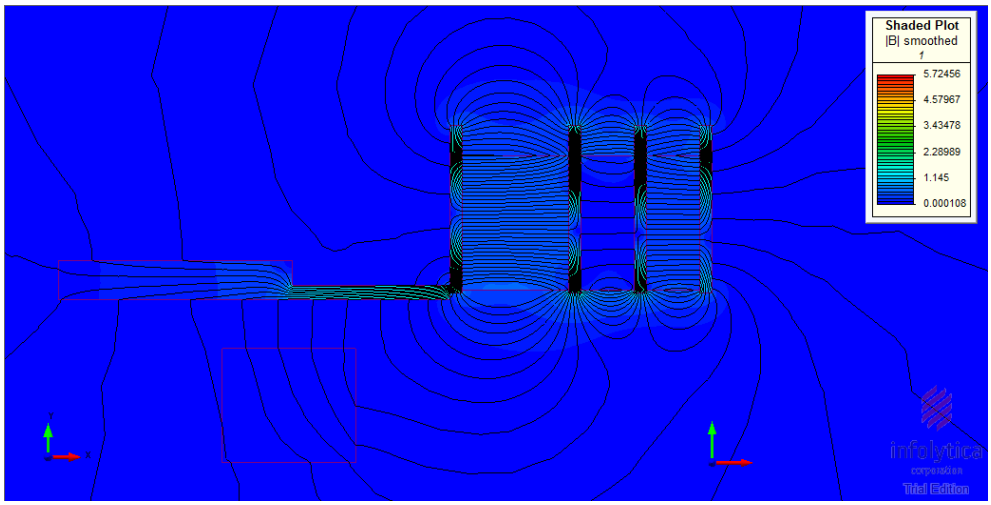

Figure 4.9: The electromagnetic solution for the original HEMPT configuration

As mentioned previously, these magnetic field models were not validated in any way. No measurements of the actual HEMPT's magnetic field were performed to allow for any validation. These models were used as a tool for shield design and as evidence of a plume shape change of the HEMPT. The main design criteria was maximum reduction of radial magnetic field outside the thruster. This reduction

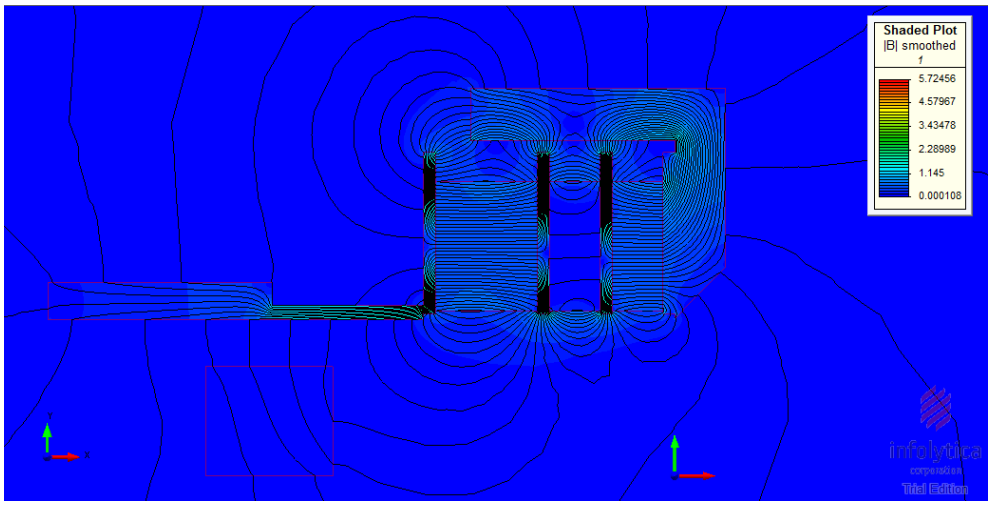

Figure 4.10: The solution for the HEMPT with selected shield configuration

is expected to decrease the amount of ions accelerated at angles to the centerline, increasing the centerline current and therefore removing the hollow plume.

5. RETARDING POTENTIAL ANALYZER

As mentioned previously, one of the main goals of this thesis is to characterize the performance of the thruster by examining the change in thrust, efficiency, and specific impulse before and after the magnetic shield is implemented, as well as visually examining the ion profile of the plume. In order to do this, a probe called a Retarding Potential Analyzer (RPA) was built. An RPA is a gridded device that filters ions in the plasma based on their kinetic energies, allowing the determination of the ion energy distribution in the plume. A discriminator grid is swept through a range of voltages, preventing ions with voltages lower than the grid voltage from reaching a collection electrode on the far side of the discriminator grid.[11, 12, 13] For this project, the RPA will be used for dual purposes. The first is to provide the ion energy in the beam to estimate the beam voltage. The second is a simple collection of ion current in the beam in order to build a profile of the thruster plume.

5.1 RPA THEORY

There are three grids in this RPA design, each with an essential function. Grid 1, or the plasma grid, closest to the opening of the probe, is left floating at the plasma potential. This minimizes perturbations between the RPA and the plasma. Grid 2 is the electron retarding grid. It is biased at negatively, repelling

the electrons and preventing them from moving further in the probe toward the collector. The final grid, Grid 3, is the discriminator or retarding grid, which is swept in the positive potential direction, selectively filtering out ions with potentials less than the grid. Ions that are able to make it past the discriminator are then collected by a collector plate and the generated current can be read by the DAQ.[11, 12, 13] Current is collected by the probe during the voltage sweep, generating a curve like that in Figure 5.1. The ion voltage distribution function $f(V)$ can be found using the relationship,

$$\frac{dI_{probe}}{dV_{probe}} = -\frac{Z_i^2 e^2 n_i A_e}{M} f(V) \tag{5.1}$$

where Z_i is the ion charge state, e is the fundamental charge, A_e is the collection area of the probe, and M is the mass of the propellant ion, in this case Xenon. This relationship can be used because the first derivative of the collected ion curve I_{probe} during a voltage sweep is proportional to the ion energy distribution $f(V)$.[11, 12, 13]

An assumption must be made that only one charge state exists in the plasma plume in order to use this relationship, however ion and Hall thrusters usually have a noticeable amount of doubly and triply charged ions. For this reason, instead of actually determining the ion energy distribution function, this relationship gives the ion voltage distribution function, which is discussed later in this chapter.[11, 12, 13]

5.2 RPA DESIGN

As mentioned, a 3 grid design was chosen for this probe. This is based off a proven RPA design used in Jameson's and others theses.[11, 12, 13] Each of the three grids was made out of a different sized stainless steel wire mesh. The

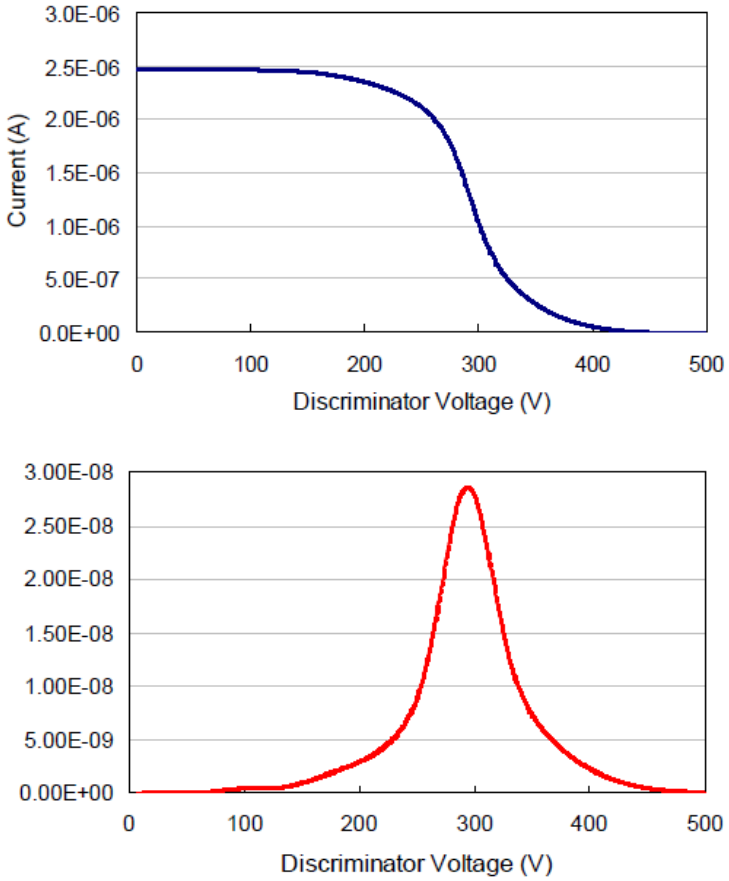

Figure 5.1: An example RPA curve and its derivative[12]

largest mesh, which had a nominal opening of 175 micrometers, was used for the floating grid. The electron retarding grid used a mesh cloth with 40 micrometer openings and the discriminator grid had a 60 micrometer mesh. A small sample of each mesh is shown in Figure 5.2. Using the images of the mesh, each of the grid transparencies, T_g, were calculated to be 0.391, 0.391, and 0.490 for the plasma, electron repelling, and ion discriminator grids respectively.

Circular discs were cut out of the meshes and spot welded to a stainless steel frame made of .02" shim stock. Teflon coated copper wires were also spot welded onto each grid and the collector. The collector was also made of .02" stainless steel shim. To space the grids, .01" and .005" thick Teflon sheet were cut into

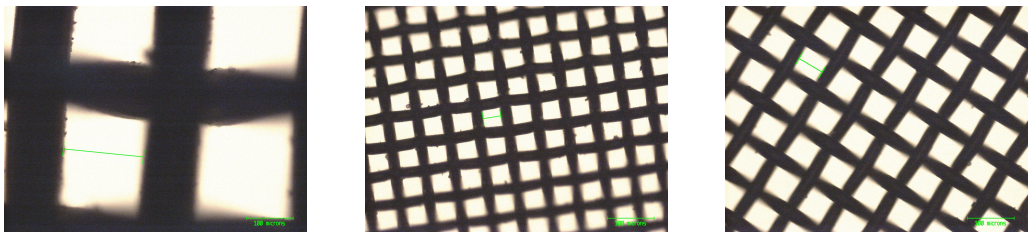

(a) (b) (c)

Figure 5.2: Images of mesh sizes (a) 175μm mesh for grid 1 (b) 40μm mesh for grid 2 (c) 60μm mesh for grid 3

rings, leaving .015" spacing between adjacent grids. The casing for the RPA was manufactured out of aluminum and connected to the common ground of the chamber. The .01" Teflon sheet was also used to isolate the grids, wires, and collectors from the RPA casing. All wires were routed along the inner Teflon sleeve to the back of the probe, where they exited the back plate through a hole that was later covered up by Kapton tape to protect the collector from excess ions. A stainless steel compression spring was inserted between the back plate and the collector to hold all the components in place. In order to promote uniform potential across the ion discriminator grid rather than a potential drop in the center of the grid, 2 mesh screens were used, spot welded to both sides of the shim ring, making the effective transparency of this grid 0.24 (0.49^2).[6] An exploded view of the Creo solid model is in Figure 5.3. The finished probe is shown Figure 5.4.

The RPA opening should direct ions straight back toward the collector. Unfortunately, when the RPA casing was first made, the orifice size was too large, about the same as the shims that hold the mesh, which would easily allow ions to collide with the non-mesh frames of the grids where they would be unable to pass through to the next area in the probe. To ensure that ions only went through the mesh part of the grid assembly, the centering ring of inner diameter 3/8" was

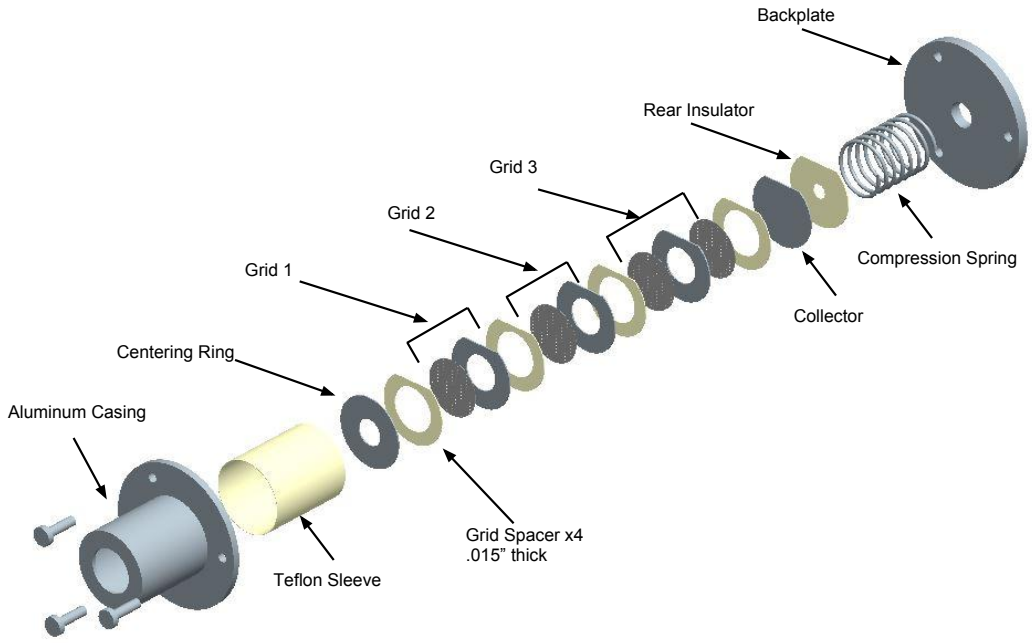

Figure 5.3: The exploded view of the RPA solid model created in Creo

(a) (b)

Figure 5.4: (a) The RPA set up on the probe drive mechanism (b) Close up of the RPA opening with the centering ring and first grid visible

added. The inner diameters of the Teflon spacers and shim rings onto which the mesh was welded are 5/8" and 1/2" respectively. Due to the Teflon spacers, the collection area of the collector electrode for use in later calculations is based off the 5/8" diameter. These dimensions are shown in Figure 5.5.

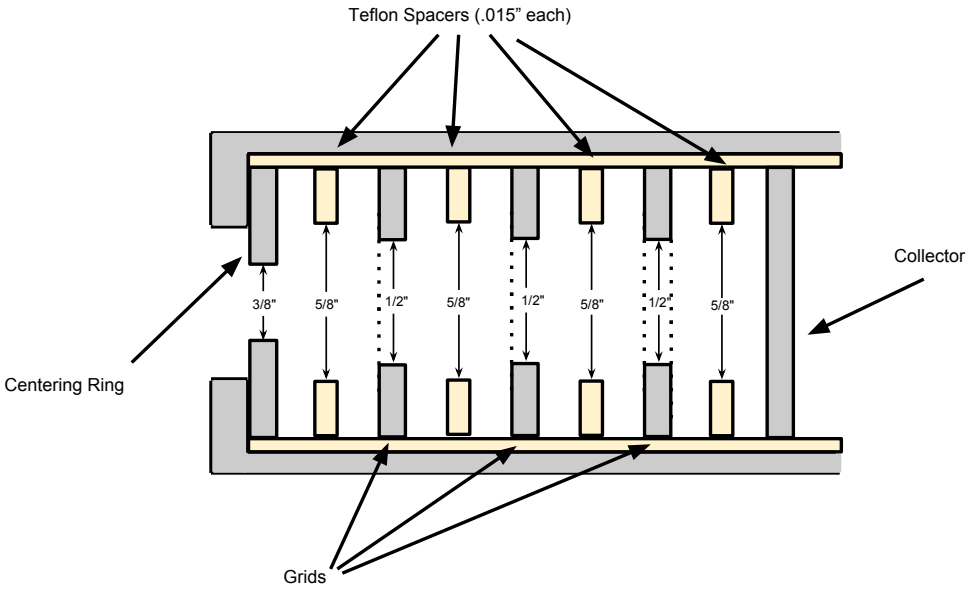

Figure 5.5: Relevant aperture dimensions of centering ring, grids, and spacers

5.3 RPA OPERATION

The standard operation of a RPA has been touched upon earlier in this chapter. The probe is positioned at a strategic place in the thruster plume. At this location, the ion retarding grid is swept through positive potentials until all ions in the beam are repelled by the grid and no current is collected by the probe. All the while, the second grid is kept at a constant negative potential (-30V) and the first grid is floating. The aluminum casing is connected to the common ground. These electrical connections can be seen in the schematic in Figure 5.6.

Using a linear probe drive, described in Section 7.1.2.1, RPA data was collected at 6 locations in the plume, spaced 1.75 inches apart. The results of the RPA data collection can be found in Chapter 8.

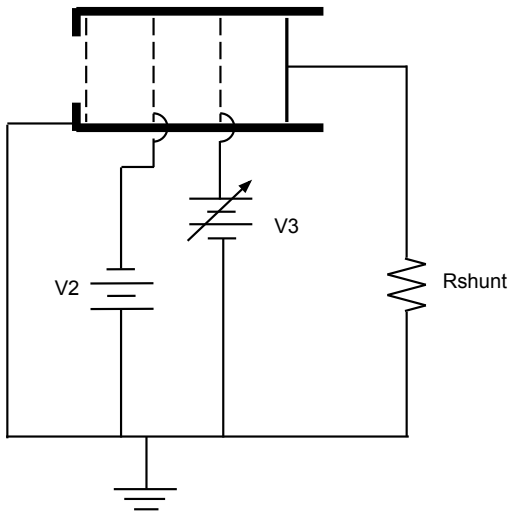

Figure 5.6: The electrical schematic for the RPA

Due to the lack of other plasma probes, the RPA was also used to build the ion beam profile. To do this, ion current was gathered by the collector for 30 seconds before a sweep of the discriminator grid voltage was initiated. Since the electron repelling grid was constant at -30V and the retarding potential was left at 0V, the maximum ion current should have been collected in this way. Collection of ion current at 11 points in the plume from the centerline to the maximum radial distance the probe could travel, 8.75", allowed a profile of the plume to be built. These 11 points were spaced 0.875" apart and the maximum angle of the included beam was 37.3 degrees from the centerline. A axisymmetric assumption allowed the profile to be mirrored about the centerline to obtain a visual representation of the entire plume. The results of this data collection are presented in Chapter 8.

5.4 RPA DATA ANALYSIS

As mentioned previously, the assumption of a single charge state in the plume changes the measured profile during a voltage sweep from the ion energy to the ion voltage distribution function. Due to this, RPA analysis provides an estimate for the beam voltage, V_b, required for thruster performance calculations. When the derivative of collected ion current curve is taken, it is proportional to the ion voltage distribution function. The voltage location of the largest peak in this function is known as the most probable ion voltage, which will be labeled as V_{RPA}. The actual beam voltage can be found from the relationship

$$V_b = V_{RPA} - \phi_p \tag{5.2}$$

where ϕ_p is the plasma potential in the beam. Unfortunately, without a second probe to provide the plasma potential, the actual beam voltage is unknown. For this reason, the most probable ion voltage will be used in the analysis as an estimate of the actual beam voltage with the knowledge that this would cause the real performance numbers to differ from those calculated in this thesis.

6. THRUSTER PERFORMANCE

6.1 PERFORMANCE METRICS

The main method of determining the effectiveness of the shield is to visualize the change in plume shape due to the implementation of the shield, however determining the performance of the thruster at each operating condition will provide useful data as well. This chapter will explain how the data collected will allow the HEMPT's performance to be determined and provide the equations used in the calculations.

The standard parameters used to describe the performance of a rocket are the thrust force produced, specific impulse, and overall efficiency. Since no thrust stand was constructed to directly measure the force of the HEMPT, the thrust will be a derived parameter through calculating the the power and ion species in the beam as well as the beam divergence. The thruster's specific impulse will be calculated using the thrust and the amount of propellant consumed. Overall thruster efficiency will combine propellant and electrical power usage of the thruster. The equations for each calculation are presented in the following section.

6.2 ANALYSIS

In order to calculate the total current in the beam, a profile of the ions in the plume must be determined. To do this the RPA is used to build up a profile of the collected ion current by the probe, I_c. This raw data is then fit to a curve that preserves the shape of the raw data points and interpolates the values in-between. An example of the collected ion current profile can be seen in Figure 6.1.

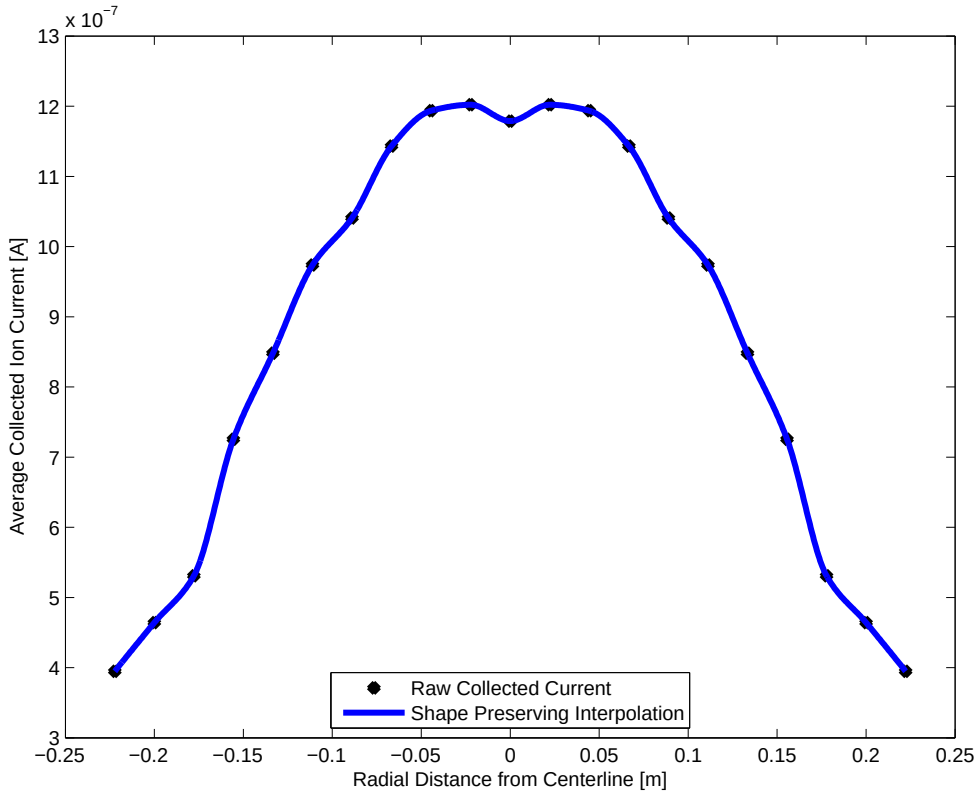

Figure 6.1: The HEMPT raw current collected by the RPA and the interpolated curve fitted to the data

This raw current can be manipulated to get the total beam current, I_b, using the equation

$$I_b = \int_0^r I(r) \cdot 2\pi \, dr \tag{6.1}$$

where $I(r)$ is the ion current in Amps as a function of radius in meters, however a few adjustments must first be made to the average collected current, I_c to get it into the correct form $I(r)$.

Since the current is collected within the RPA, the ions must travel through the RPA orifice and all three grids before it can be collected. This means that the collected current must be divided by the net grid transparency, T_g as well as the area of the probe orifice, A_{RPA}, though this is not the only correction that must be considered.

During the trip from the thruster to the probe, the charged particles interact with other neutral gas particles in the chamber. The high base pressure in the chamber leads to charge exchange (CEX) in the plasma plume. This CEX will cause a reduction in the measured current at the probe. To account for this, a correction factor must be used.[8, 9, 21]

In this analysis, a simplified model for only singly charged ions was used from Shastry et al.[21] The CEX correction factor for singly charged ions, $(j/j_0)_{Xe^+}$, can be found using

$$(j/j_0)_{Xe^+} = \exp(-n_0\sigma_1 z) \tag{6.2}$$

where n_0 is the neutral density in the chamber in particles per cubic meter, z is the distance from the thruster to the probe in meters, and σ_1 is the effective cross sectional area of the charged particle in square meters. σ_1 can be calculated in Å^2 by the equation

$$\sigma_1 = 87.3 - 13.6\log(0.8V_d) \tag{6.3}$$

where V_d is the discharge voltage in volts, and then converted to square meters for use in Equation 6.2.[8, 21]

With all of these corrections, the actual current as a function of radius, $I(r)$

can now be determined from the raw current collected with the equation

$$I(r) = \frac{I_c}{A_{RPA} T_g (j/j_0)_{Xe^+}} \tag{6.4}$$

where A_{RPA} is the orifice area of the RPA in square meters. $I(r)$ can then be utilized to find the beam current, I_b through Equation 6.1.

Next, the RPA is operated at several places within the plasma plume. The RPA data at a single location is a plot of the collected current as a function of discriminator grid voltage. Taking the derivative of the current with respect to voltage provides an estimate of the most probable beam voltage, V_b, which can be found at the peak of the current derivative. Unfortunately during testing, the RPA curves collected were discarded due to an unknown delay in the collected current, causing a lack of confidence in the collected data. Due to this, the beam voltage will instead be estimated by using the relationship

$$V_b = 0.75 V_d, \tag{6.5}$$

in other words, the beam voltage fraction of discharge, shown in Equation 6.10 is defined to be 75%. The discarded RPA curves are discussed more in the Results chapter, Chapter 8.

An important parameter of electric propulsion thrusters is the half-angle divergence of the plasma plume. The divergence angle, θ, changes based on the definition chosen. For example, the angle can be defined by enclosing a certain percentage of the beam current, finding the full width at half-maximum (FWHM), or by performing some sort of current weighting. For this project, the divergence half-angle was defined as 95% enclosure of the calculated beam current. This value has been used by Hofer and others in Hall thruster experiments.[11]

Despite trying to best simulate the actual space environment during thruster testing, a vacuum chamber will always have differences that should be taken

into account. One of these is ingestion. Since the thruster is tested in a finite volume and propellant is constantly being injected into the system, the vacuum pump needs to remove all that gas. In space, used propellant has the whole of the universe to expand into, however in a small confined chamber, some of that gas will be re-used by the thruster if not immediately removed by the pump, artificially improving thruster performance in way that cannot not happen on-orbit.[9] In order to account for this ingestion, the mass flow rate of propellant used in performance calculations must be adjusted. The total flow rate in SCCM, Q_{total}, is the addition of the injected and ingested propellant,

$$Q_{total} = Q_{injected} + Q_{ingested} \tag{6.6}$$

both of which are in units of SCCM.[9] The injected flow is the propellant going into the HEMPT and hollow cathode, while the ingested flow can be calculated using

$$Q_{ingested} = 7.82 \times 10^{8} \frac{P \cdot A \cdot \eta_c}{\sqrt{T \cdot M_{Xe}}} \tag{6.7}$$

where P is the pressure in the chamber in Torr, A is the open area of the thruster in square meters, η_c is a correction factor for conductance into the thruster, T is the neutral gas temperature in Kelvin, and M_{Xe} is the mass of a Xenon ion in kilograms.[9] The conduction correction factor, η_c, will be assumed 1. The open area fraction is usually just the area of the channel, however recent developments have shown that since ion acceleration occurs outside the thruster as well, the effective open area is larger.[8] For this reason, A in this equation will be calculated as the area of a hemisphere with radius equal to that of the channel. Using these values, and the conversion between SCCM and kg/s for Xenon, the corrected mass flow rate, $\dot{m}_p$ in kilograms per second is[9]

$$\dot{m}_p = 9.83009 \times 10^{-8} Q_{total}. \tag{6.8}$$

Although a specific amount of power is put into the thruster, not all of that power shows up in the ion beam. Inefficiencies will always cause a certain amount of power loss to the environment. Both power and propellant are put into the thruster for operation, however how well these are utilized by the system determine the overall efficiency of the thruster. Several individual ratios and efficiencies go into determining the total thruster efficiency.

The beam current fraction of the discharge, η_b, can be found with the equation

$$\eta_b = \frac{I_b}{I_d} \tag{6.9}$$

where I_b is the beam current determined in Equation 6.1 and I_d is the discharge current from discharge power supply, both in Amps.[9] Similarly, the beam voltage fraction of discharge, η_v, is determined through

$$\eta_v = \frac{V_b}{V_d} \tag{6.10}$$

where V_b is the beam voltage and V_d is the voltage from the discharge supply, both in volts.[9]

The amount of ionized propellant also has an effect on overall efficiency, therefore thruster mass utilization efficiency, η_m, must be calculated with the equation[9]

$$\eta_m = \alpha_m \frac{I_b \cdot M_{Xe}}{\dot{m}_p \cdot e} \tag{6.11}$$

where e is the elementary charge in Coulombs and α_m is a term that accounts for doubly charged ions in the beam, calculated by

$$\alpha_m = \frac{1 + \frac{1}{2}\frac{I^{++}}{I^{+}}}{1 + \frac{I^{++}}{I^{+}}} \tag{6.12}$$

where $\frac{I^{++}}{I^{+}}$ is the fraction of double ion current in the beam[9], assumed to be 5% in this thesis.[17]

Unfortunately not all of the electrical energy put into the system shows up in the beam. Some of the energy is lost to heat and some must go into plasma generation in the cathode. The electrical efficiency, η_o can be determined by

$$\eta_o = \frac{I_b \cdot V_b}{I_b \cdot V_b + P_k} \tag{6.13}$$

where P_k is the power to the keeper in Watts.[9]

The thrust correction factor, α corrects for doubly charged ions in the beam. It can be calculated with the equation[9]

$$\alpha = \frac{1 + 0.707\frac{I^{++}}{I^{+}}}{1 + \frac{I^{++}}{I^{+}}}. \tag{6.14}$$

The total thrust correction factor, γ, can then be calculated using the thrust correction factor and the divergence angle[9]

$$\gamma = \alpha \cos\theta. \tag{6.15}$$

A combination of all the previously determined efficiencies gives the total thruster efficiency, η_T,[9]

$$\eta_T = \gamma^2 \eta_b \eta_v \eta_m \eta_o. \tag{6.16}$$

Finally, the actual force of thrust of the HEMPT, T, can be determined using the equation[9]

$$T = 1.65\gamma I_b \sqrt{V_b} \quad [\text{mN}]. \tag{6.17}$$

The specific impulse of the thruster, I_{sp}, is a ratio of the thrust and propellant usage, and can be found using the relationship[9]

$$I_{sp} = \frac{T}{\dot{m}_p \cdot g_0}. \tag{6.18}$$

These last few equations, 6.16, 6.17, and 6.18, are used to determine the three performance parameters used as a comparison of the thruster with and without the shield, which is detailed in the Results chapter, Chapter 8.

7. HEMPT TESTING

7.1 FACILITIES AND APPARATUS

7.1.1 VACUUM CHAMBER SYSTEM

Testing for this thesis was performed in the Aerospace Engineering department's Space Environments Laboratory located on the Cal Poly campus. A High Vacuum Equipment Corporation (HVEC) 350 liter bell jar vacuum was used along with a Welch 1374 Duo-Seal Vacuum Pump and a CTI-Cryogenics Cryo-Torr 8 High Vacuum Pump run by a Model 1020R Compressor. The bell jar measures 30 inches in diameter and approximately 30 inches high. This is the largest vacuum chamber available in the Space Environments lab and thus the ideal chamber for this thesis due to the necessity of performing plume measurements. A large diameter bell jar allowed plenty of room for the plasma plume to develop without chamber wall impingement and therefore enough space for the diagnostic probe to move through the plume 1 foot downstream of the thruster. The vacuum chamber system is shown in Figure 7.1.

The vacuum system utilizes the Welch mechanical pump to obtain medium vacuum ($1x10^{-3}$ to 25 Torr) inside the chamber, then switches over to the cryo pump to reach high vacuum ($1x10^{-9}$ to $1x10^{-3}$ Torr). At the time of testing, a base pressure lower than the maximum allowable pressure of $5x10^{-6}$ Torr was

Figure 7.1: The HVEC vacuum system used for HEMPT testing

achieved before initiating cathode heating and Xenon gas flow into the chamber. Keeping the base pressure lower than this value prevents the impurities in the air from contaminating the hollow cathode and poisoning the insert rendering it useless.[14] The schematic for the HVEC vacuum system is shown in Figure 7.2.

The pressure in the chamber is measured by a Granville Phillips 275 convectron gauge at medium vacuum and a Bayard-Alpert 274 ion gauge at high vacuum. Both gauges are controlled by a Granville Phillips 307 Vacuum Gauge Controller. During thruster operation, the pressure reading on the ion gauge must be divided by 2.87 in order to obtain true pressure because of the Xenon gas present in the chamber.

In order to prevent the highly energetic ions in the thruster plume from sputtering the stainless steel walls of the chamber, the top half of the chamber was

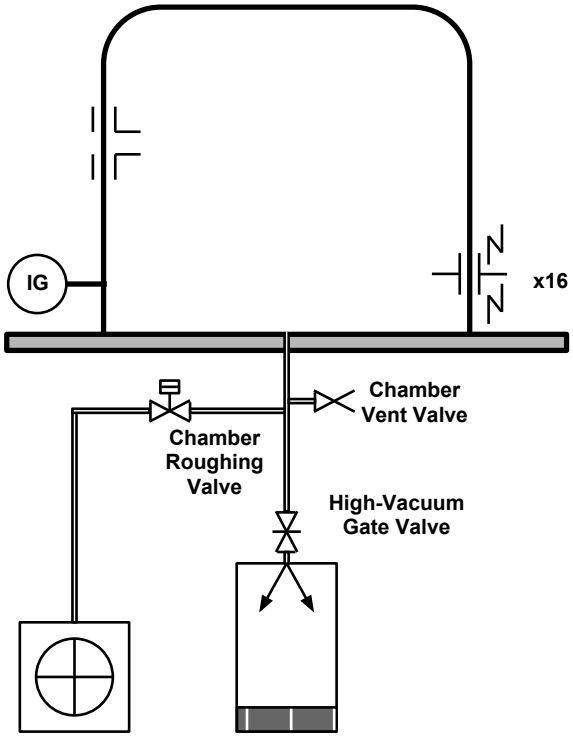

Figure 7.2: Schematic for the HVEC vacuum system used for HEMPT testing

lined with 1/8 inch thick PAN carbon felt. The felt was also placed over the probe drive support structure to protect the thruster ceramic from aluminum backsputter as well as protect the probe drive mechanism from the plasma.

7.1.2 DIAGNOSTIC SYSTEM

7.1.2.1 PROBE DRIVE

A probe drive was constructed for the purposes of this thesis. With t-slotted aluminum framing as a base, a bipolar stepper motor was used to drive two

acetal pulleys connected with a Urethane timing belt. The RPA was clamped to the timing belt and guided along two stainless steel rails. This probe drive system can be seen in Figure 7.3.

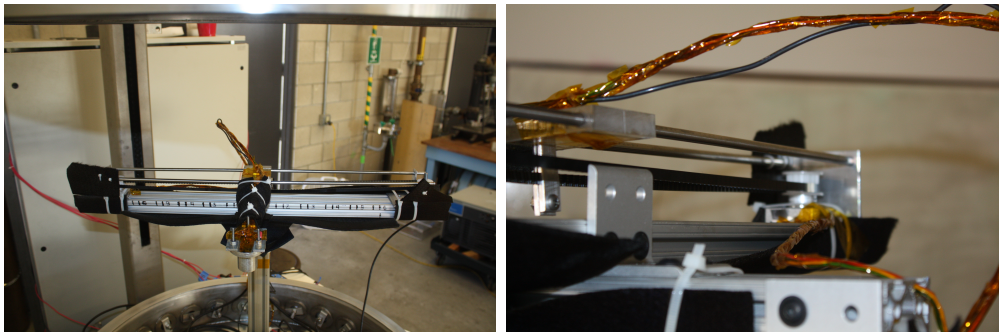

(a) (b)

Figure 7.3: (a) The probe is driven by a stepper motor with a timing belt across steel rails (b) A closer look at the drive mechanism

The stepper motor was controlled using an Arduino Uno microcontroller and a EasyDriver stepper motor driver board, which were powered using an Extech Instruments 18V-3A DC power supply. The stepper motor driver was set up for the motor to operate in 1/8th step mode, where it takes 1600 steps to make a full revolution. Due to the selected timing belt, which has a pitch of 0.2", a full revolution of the motor shaft results in 2.8" linear motion of the probe drive.

During data collection for the RPA curves, the probe was positioned in 6 evenly spaced locations, each 1000 steps apart, or 1.75". These positions are marked by the X's in Figure 7.4. As the figure shows, RPA data was only collected on one side of the thruster due to an axisymmetric assumption of the plasma plume.

To build the current profile, the RPA was positioned at each of the 6 locations in Figure 7.4 plus a location halfway between those 6, for a total of 11 locations.

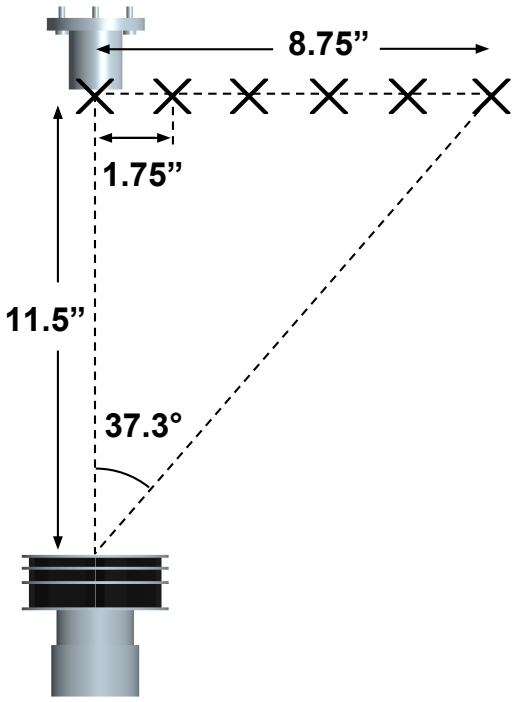

Figure 7.4: The 6 locations of RPA data collection, spaced 1.75” apart from the thruster centerline to the outer limit of the probe drive

7.1.2.2 DATA COLLECTION

The Student Edition of LabVIEW 2012 along with a NI 9205 DAQ were used for data collection in this thesis. When operating the RPA, the data acquired included the discriminator grid voltage and the current collected. The DAQ had a voltage input range of ±10V. To prevent the discriminator grid, which is swept upwards of 700 volts, from destroying the DAQ, a voltage divider was used. Resistors were selected from readily available equipment. The voltage divider included R_1 and R_2, which had values of 18.96kΩ and 104.3Ω respectively. A shunt resistor was placed in series with the RPA collector for the DAQ to read the voltage across. This shunt resistor, R_c, had a value of 1.46MΩ. This magnitude of resistance was chosen so that current on the order of 1μA would allow the

DAQ to read several volts, but still under the 10V maximum input. During the first several tests however, the data collected was almost purely noise, with no discernible curve. To eliminate this issue, a low-pass filter was added across the shunt resistor. This filter included R_f, with a value of 10kΩ and a capacitor, C_c which had a value of $10\mu F$. The voltage divider and shunt resistor configurations can been seen in Figure 7.5.

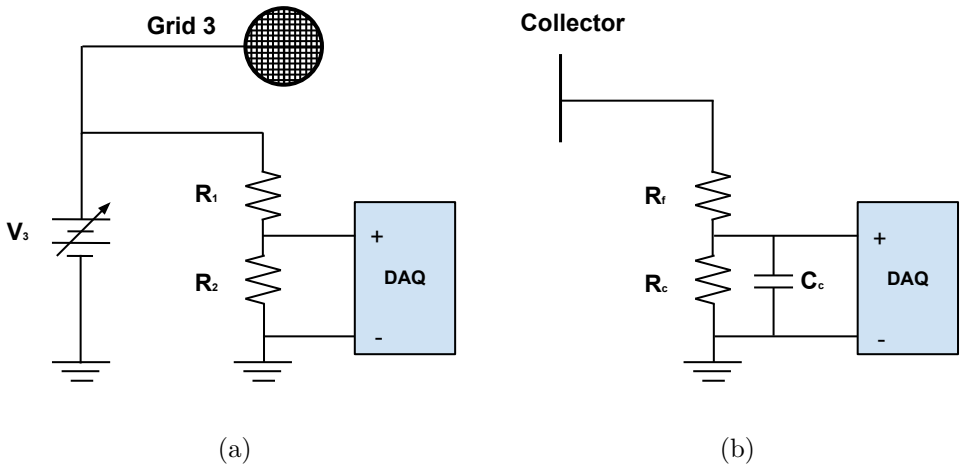

(a) (b)

Figure 7.5: (a) Schematic for the voltage divider circuit used on the discriminator grid (b) Schematic for the shunt resistor circuit used on the collector electrode

7.1.3 PROPELLANT SYSTEM

The propellant system used during HEMPT testing is detailed in this section. The components used were a Xenon propellant tank, a stainless steel two-stage pressure regulator, two shut-off valves, two needle valves, two propellant flow meters, two gas feedthroughs, and two propellant isolators, all connected with stainless steel tubing and Swagelok connections.

Ultra High Purity (UHP) Xenon gas was obtained for electric propulsion projects in the Space Environments Lab such as the HEMPT testing. This means

that the Xenon is 99.999% pure. The propellant must be at least UHP to prevent poisoning of the hollow cathode insert.[14] In order to maintain purity of the Xenon gas through the system, the pressure regulator was a stainless steel two-stage high purity regulator, made by Smith Equipment. This regular has an outlet pressure range of 0-30psig. Both flow meters were OMEGA FMA-A2300 with digital readouts, in units of standard cubic centimeters per minute (SCCM). These flow meters are calibrated for Nitrogen gas, and therefore the readout must be multiplied by a factor of 1.44 to obtain the true flow rate of Xenon, with an accuracy of $\pm 4\%$.[4] Unfortunately, these flow meters had not been calibrated for several years outside their acceptance date, which provides a large uncertainty about the actual propellant flow into the chamber. This is discussed more in the results section.

Each propellant line going into the chamber has a Swagelok SS-4H bellows-sealed valve to shut-off flow to the thruster or cathode when not in use, as well as a VACOA MV-25 precision micrometer gas metering valve to control the flow rate of Xenon into the components.

Inside the vacuum chamber, both the thruster and hollow cathode propellant lines include an electrical isolator to prevent the components from forming an electrical connection with the grounded chamber. The discharge line was wrapped in a plastic insulator from the thruster to the propellant isolator to prevent plasma in the chamber from ionizing propellant before it reached the thruster. A schematic of the propellant system shown in Figure 7.6, while the actual system is shown in Figure 7.7.

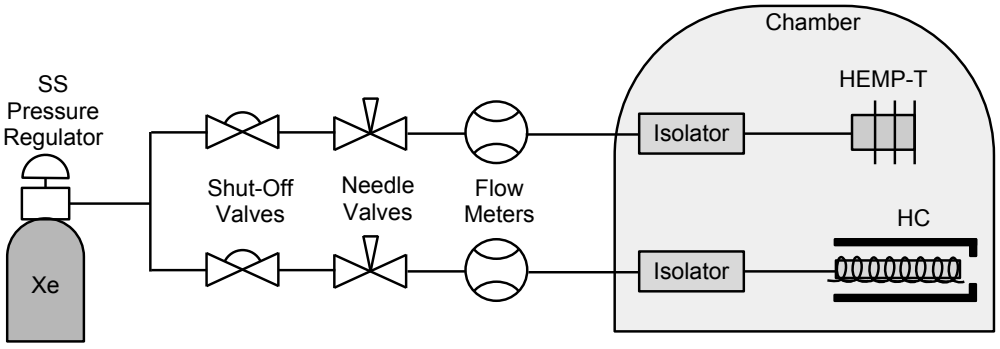

Figure 7.6: The propellant system and components used for HEMPT testing

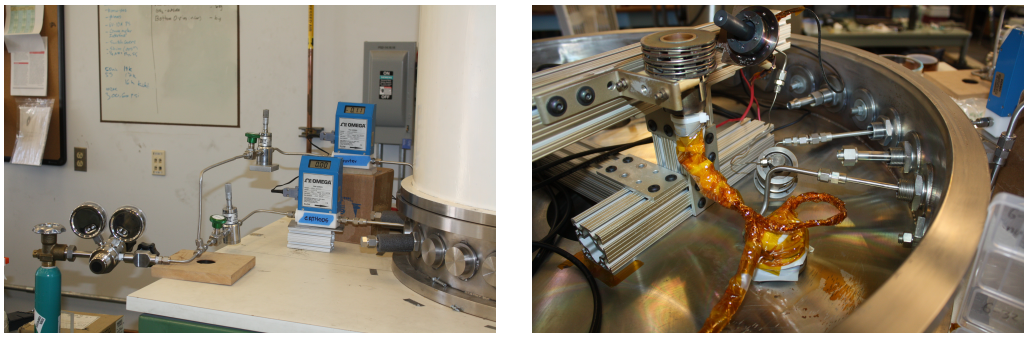

(a) (b)

Figure 7.7: (a) The propellant system outside the chamber, including the Xenon tank, pressure regulator, shut-off valves, needle valve, and flow meters (b) The propellant system inside the chamber, including the propellant isolators, HEMPT and hollow cathode

7.1.4 ELECTRICAL SYSTEM

The vacuum chamber system includes 8 coaxial feedthroughs; 5 N-type and 3 TNC, allowing for electrical signals to be passed into the chamber. Unfortunately, the amount of isolated electrical feedthroughs into the chamber required for the entire system was 11: 4 for the motor coils, 4 for the RPA, 2 for the hollow cathode (heater and keeper), and 1 for the thruster discharge. Since not enough

feedthroughs were available, a thermocouple feedthrough with greater than 20 thermocouples was used for the RPA electrical signals. Four of these thermocouples were instead used for the electrical current of the 3 grids and collector. The maximum current any of these wires see is on the order of microamps, therefore the re-purposed thermocouple wire was able to fully handle the task.

Due to the complexity of the electrical system for EP thrusters, a total of 6 power supplies were utilized. These power supplies and their outputs can be seen in Table 7.1. The Glassman power supply was used for two purposes. First it was used in order to help ignite the hollow cathode keeper. The hollow cathode often required greater than 500V before plasma generation was initiated, and since the keeper supply's maximum voltage output was around 314V, the voltage was augmented with the Glassman. Diodes were placed in the proper locations between the keeper and Glassman supplies for protection. Second, the Glassman was used to provide the retarding potential on the discriminator grid in the RPA.

Table 7.1: Power supplies used for HEMPT testing

Power Supply	**Model**	**Output**
Keeper (V_k)	Agilent N5771A	0-300V, 0-5A
Heater (V_h)	HP 6038A	0-60V, 0-10A
Discharge (V_d)	Sorenson XG 300-5.6	0-300V, 0-5.6A
Igniter (V_i)/Grid 3 (V_3)	Glassman FC1P120	0-1000V, 0-125mA
Grid 2 (V_2)	Instek GPS 2303	0-30V, 0-3A
Probe Drive (V_{pd})	Extech Inst. 382202	0-18V, 0-3A

The electrical schematic for the entire thruster and probe system can be seen in Figure 7.8. The switch, S_i was used to switch the Glassman between igniter and grid 3 after the cathode was lit and data collection was about to begin. Every

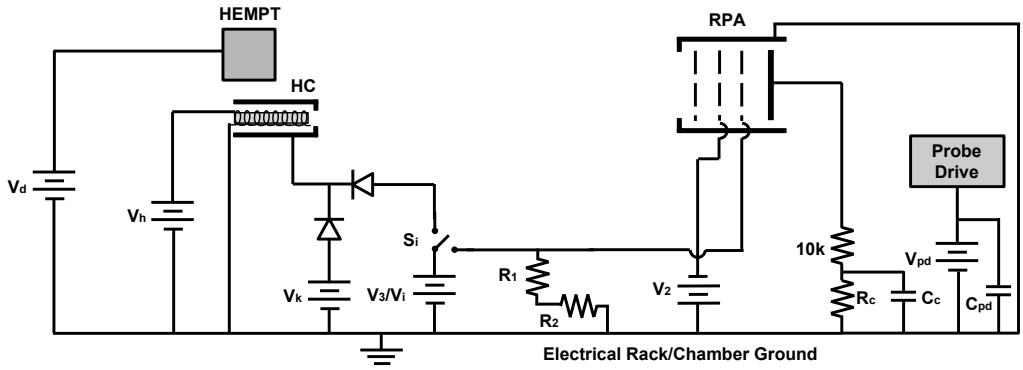

Figure 7.8: The electrical schematic used for HEMPT testing

power supply was connected to the common ground, which included the vacuum chamber and the electrical rack.

Many of the wires required electrical isolation inside the chamber. The discharge line going to the HEMPT anode was wrapped in many layers of kapton and Teflon sheet. Without this isolation, the plasma from the cathode would be attracted straight to the line, which is at a high positive potential, burning it and bypassing the thruster which would not work properly. In addition to the discharge line, the discriminator voltage (grid 3) line was wrapped for similar reasons. That line is swept from 0-600+V, which would also attract the plasma if not properly isolated.

Many attempts at running the thruster revealed that the probe drive system was extremely sensitive to electrical interference and noise. The motor often did not work properly while the thruster was running due to the presence of plasma and other noisy electrical signals into the chamber. To help prevent this problem, the motor coil wires, along with the motor, were all wrapped tightly in aluminum foil which was grounded to the common ground. The probe drive was encased in an acrylic box which was then wrapped in foil. This was done in

hopes of shielding these wires and components from any noise in the system in order to allow proper operation of the probe drive system. While this method provided enough shielding to obtain all the data, the probe drive still operated reluctantly and provided some difficulties in maneuvering the probe to the correct locations. The lines and probe drive wrapped in foil can be seen in Figure 7.9. Some suggestions on how to improve the probe drive have been detailed in the Lessons Learned section, Appendix A.

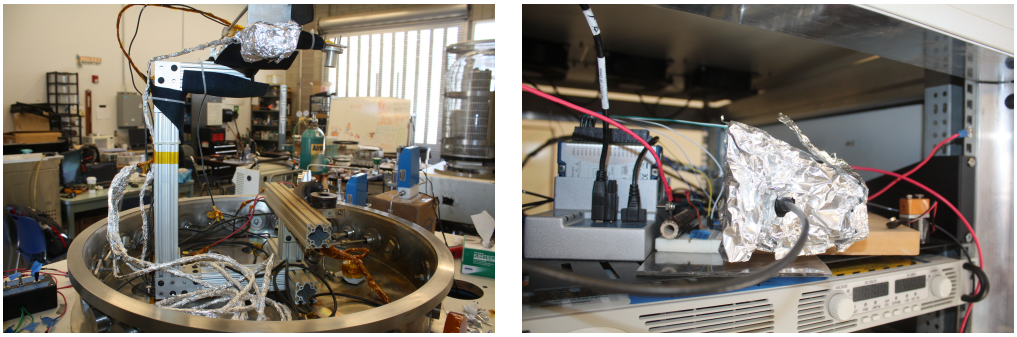

(a) (b)

Figure 7.9: (a) Foil wrapped over the motor coil lines and motor (b) Foil covering the probe driver and microcontroller circuit boards

7.2 TESTING

7.2.1 HEMPT OPERATION

In order to provide consistent results, it was attempted to run the HEMPT at the same operating conditions before and after the implementation of the shield. Unfortunately, this was not possible due to issues that will be discussed more in Chapter 8.

It took many attempts running the HEMP-thruster before smooth and stable operation was achieved. One stable operating condition for the HEMPT was

found by making adjustments in HEMPT flow, cathode flow, discharge voltage, and cathode keeper current during these first few tests. No useful data was recorded in these first tests due to issues with the data acquisition system and noise, however several of these tests were required to learn how to operate the thruster anyway. This stable operating condition became the nominal parameters at which each test was run, which are presented in Table 7.2.

Table 7.2: Nominal operating conditions of the HEMPT during testing

Parameter	**Operating Condition**
HEMPT Flow Rate	4.49 ± 0.18 SCCM
Cathode Flow Rate	2.87 ± 0.11 SCCM
Discharge Power	200.9 ± 0.1 V, 1.6 ± 0.1 A
Keeper Power	24.3 ± 0.1 V, 2.3 ± 0.1 A

8. RESULTS

This section will present the results of the HEMP thruster testing at Cal Poly. Calculations in this section will follow the analysis presented in Section 6.2 except where explicitly stated.

As mentioned briefly in Section 6.2, the actual RPA curve data was discarded. This data would have been used to determine the most probable beam voltage through an examination of the ion energy distribution as explained in Chapter 5. In a proper RPA data collection, no ion current will be collected beyond a retarding potential 100V or so greater than the discharge voltage. While operating the thruster at a discharge of 200V and sweeping the retarding potential upwards of 600V, significant current was being recorded on the collector at these high retarding potentials. It was also noted that a delay of 20 or so seconds was present between the time the grid potential was increased to a certain value and when the collector current would settle upon its value. For example, if the discriminator grid potential was increased from 0 to 15 volts in 3 seconds, the collector current would continually drop and finally settle 20-30 seconds later. This destroyed any confidence in the actual RPA data and therefore it was all discarded. As mentioned in Section 6.2, the beam voltage will instead be estimated as 75% the discharge voltage. To prevent this problem from being an issue during ion profile building, the probe was left to sit at its location for 30-60 seconds before 30 seconds of data was taken and averaged. During the wait period,

the collected current would settle on a fixed value, which was then used to build the plume profile.

8.1 HEMPT RESULTS

After many difficulties during the testing process, the entire setup finally worked together and data was collected. The thruster was run as shown in Figure 8.1. The RPA was used with a 0V discriminator grid potential and data was collected and averaged in order to build the profile of the ions in the beam. The average collected ion current, I_c, is presented in Figure 8.2.

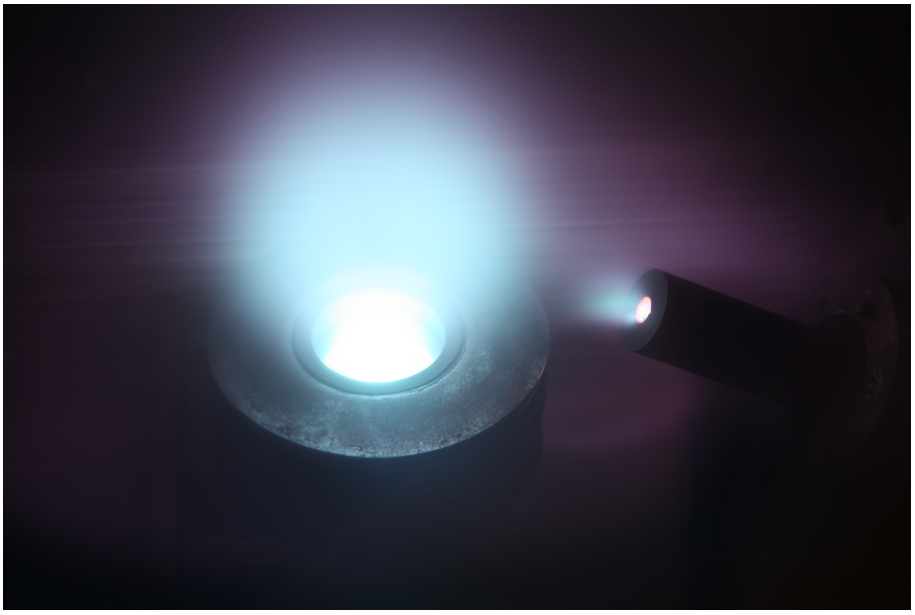

Figure 8.1: Picture of the HEMPT during operation

The plume shape was created using an interpolation fit that preserved the shape of the original data. Figure 8.2 does present a hollowness in the plume in the form of reduced centerline ion current, although this hollow shape is not as extreme as expected. It was hypothesized earlier that the maximum ion current would be found 15 to 20 degrees off the centerline, based off a visual of the

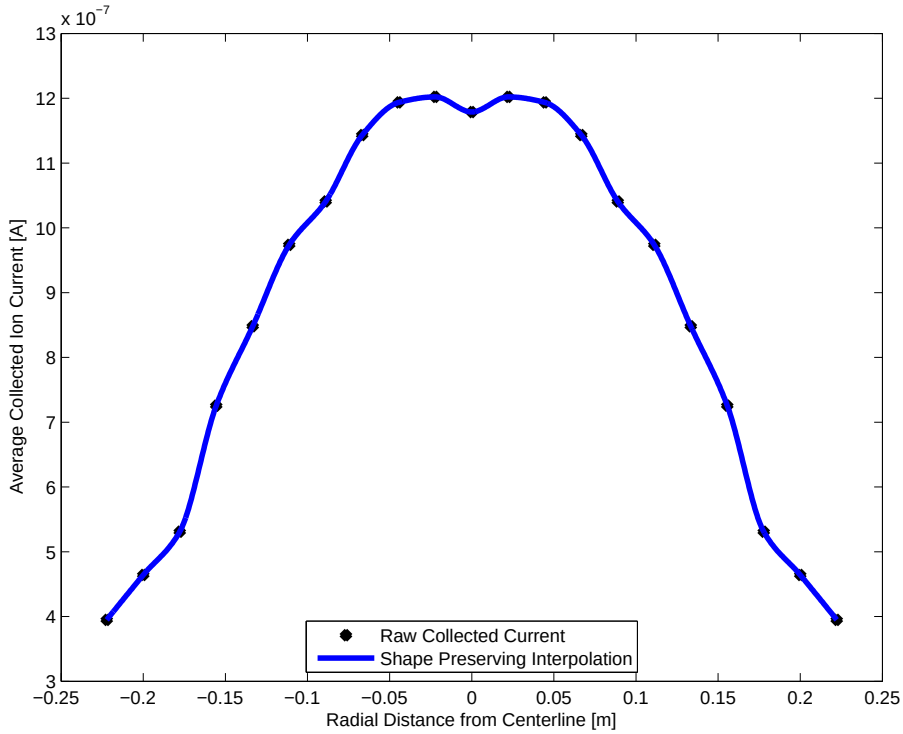

Figure 8.2: The HEMPT's ion plume shape showing reduced centerline current, or a "hollow" plume

HEMPT plume. The collected current puts this peak at approximately a 4.5 degree offset, however, which is much closer than expected. In addition, the centerline ion current only has about a 2% reduction from the peak ion current. Again, this is less extreme than hypothesized.

The fitted curve was then used to determine the beam current, I_b. The CEX correction factor was found to be 0.3241 using Equation 6.2, the net grid transparency was determined to be 0.0366, and the open area of the RPA was determined to be 7.56x10^{-5} m^2 estimating a 3% larger diameter due to effects of drilling a thin metal sheet.[8] Using these parameters in Equations 6.4 and 6.1, the beam current I_b was determined to be 1.39 A. This was then corrected again to account for an estimated 10% neutral depletion in the beam due to ionization[8],

so the final beam current was 1.25 A.

Using the calculated beam current and moving forward in the performance analysis, it becomes clear that the mass utilization efficiency calculated with Equation 6.11 is too high, at 1.94. Mass utilization is an efficiency that should be less than 1, since it describes how much of the propellant is ionized. This incorrect calculation is likely because of large error in the gas flow into the chamber.[8] To deal with this issue, a correction factor was introduced. This assumed correction factor of 0.5 was adjusted until the mass utilization was under 1. Both mass utilization efficiency and specific impulse calculations must be multiplied by this correction in order to obtain reasonable performance numbers. A major assumption is made here, introducing this correction factor. It is used in order to adjust the performance parameters of the thruster to obtain reasonable values. Without the correction, specific impulse and efficiency for the HEMPT are calculated to be 2460 sec and 58% respectively. Neither of these numbers are reasonable for the operating parameters of the HEMPT, in fact they are highly inflated. The source of this error must be determined in the future, however the correction factor is used during this thesis instead. Before more testing begins, a calibration of the pressure measurement and flow equipment must be performed in order to remove the need for this correction factor, however this was not able to be done for this project.[8] The final performance values for the HEMPT thruster before the implementation of the shield and with the correction factor are presented in Table 8.1.

Errors for each parameter have been included in the calculated performance. As mentioned in the preceding paragraph, there is much uncertainty in the actual amount of propellant in the system. This creates a large error in certain parameters affected significantly by propellant flow, including mass utilization efficiency

Table 8.1: The calculated final performance values of for the original HEMPT configuration at nominal operating conditions

Calculated Performance Parameter	Value
Beam Current, I_b	1.25 ± 0.14 A
Mass Flow Rate, $\dot{m}_p$	8.53 ± 0.42 x10^{-7} kg/s
Beam Divergence Half-Angle, θ	34.3 degrees
Beam Current Fraction of Discharge, η_b	78% ± 9%
Beam Voltage Fraction of Discharge, η_v	75% [defined parameter]
Mass Utilization Efficiency, η_m	97% ± 12%
Electrical Efficiency, η_o	77% ± 2%
Total Thrust Correction Factor, γ	0.814
Thrust, T	**20.4 ± 2.4 mN**
Specific Impulse, I_{sp}	**1230 ± 154 sec**
Total Thruster Efficiency, η_T	**29% ± 5%**

and specific impulse. Unfortunately, without more precise measurement of flow and pressure in the system, these errors will remain large.

8.2 SHIELDED HEMPT RESULTS

After successfully determining the plume shape of the original HEMPT configuration, the iron shield was added to the thruster face as shown in Figure 8.3.

An attempt was made to run the thruster at the same operating conditions at the original HEMPT, specified in Table 7.2, however this was not possible. The shielded HEMPT discharge current was much higher and the discharge voltage much lower than the nominal operating conditions. Data was then collected in

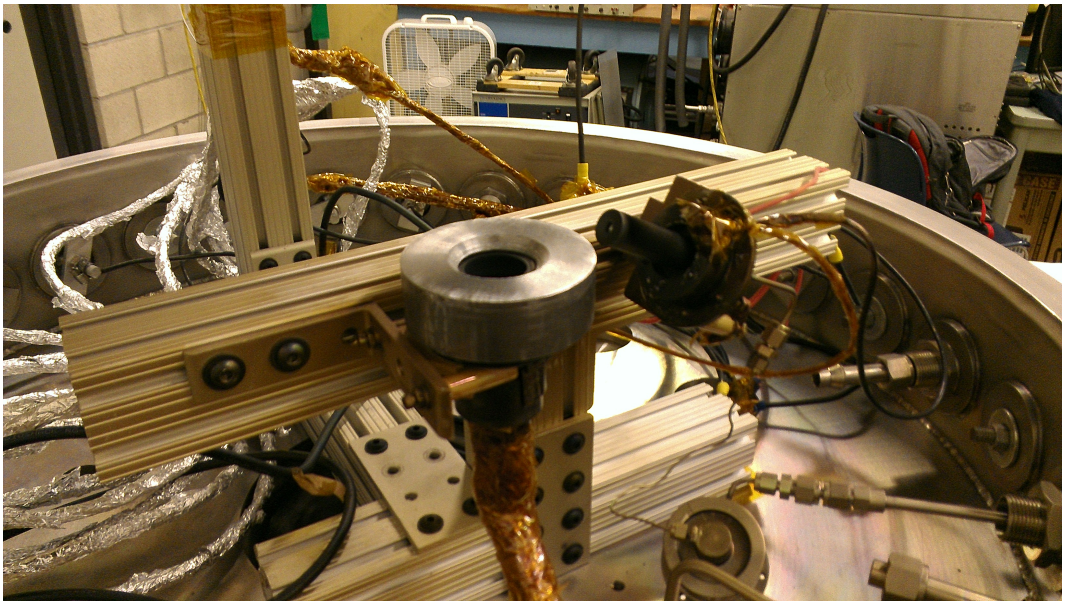

Figure 8.3: The HEMP-thruster with iron shield incorporated. The shield is held onto the thruster by the existing magnets

the shielded HEMPT's ion plume at the operating conditions in Table 8.2.

Table 8.2: Operating conditions of the shielded HEMPT during testing

Parameter	Operating Condition
HEMPT Flow Rate	4.51 ± 0.18 SCCM
Cathode Flow Rate	2.85 ± 0.11 SCCM
Discharge Power	100.0 ± 0.1 V, 3.4 ± 0.1 A
Keeper Power	16.0 ± 0.1 V, 2.3 ± 0.1 A

Under these operating conditions, the shielded HEMPT was run and the RPA was utilized to collect data at the same points as the original test. The operating shielded thruster is pictured in Figure 8.4, while the plume shape is presented in Figure 8.5.

As shown in Figure 8.5, the implementation of the shield onto the thruster

Figure 8.4: A picture of the shielded HEMPT during operation

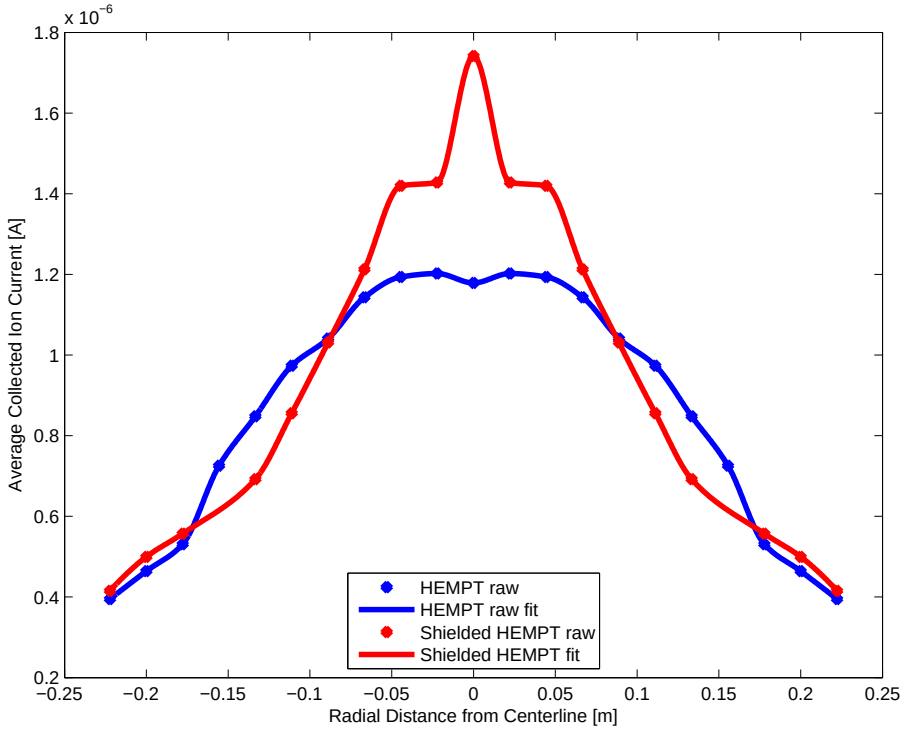

Figure 8.5: The shielded HEMPT's ion plume shape with increased current at the centerline, compared with the original plume shape

did fix the hollow plume issue. The centerline current increased from 1.18μA to 1.74x10μA, a percentage increase of almost 48%. The new plume shape of the HEMPT includes a "shoulder" off the centerline. It is believed that this

particular data point was subject to a misplacement of the probe, further away from the centerline than expected which produced a lower collected ion current. It is unlikely the actual plume follows this odd shape, however the data is presented as collected.

Unfortunately and unexpectedly, during the process of reshaping the plume with the shield, the performance of the thruster decreased significantly, evidenced in Table 8.3.

Table 8.3: The calculated final performance values for the shielded HEMPT configuration, showing a decrease in overall performance

Calculated Performance Parameter	**Value**
Beam Current, I_b	1.43 ± 0.18 A
Mass Flow Rate, $\dot{m}_p$	8.53 ± 0.42 x10^{-7} kg/s
Beam Divergence Half-Angle, θ	34.4 degrees
Beam Current Fraction of Discharge, η_b	42% ± 5%
Beam Voltage Fraction of Discharge, η_v	75% [defined parameter]
Mass Utilization Efficiency, η_m	111% ± 15%
Electrical Efficiency, η_o	74% ± 2%
Total Thrust Correction Factor, γ	0.814
Thrust, T	**16.6 ± 2.0 mN**
Specific Impulse, I_{sp}	**991 ± 132 sec**
Total Thruster Efficiency, η_T	**17% ± 3%**

Before testing, it was speculated that the shield would provide both an increase in centerline ion current and a narrowing of the plume, the second of which would be represented by a decreased half-angle divergence. Calculations

show that the plume divergence experienced almost no change at all due to the shield, keeping the value around 34 degrees. Visually, Figure 8.5 shows a narrowing before approximately 27 degrees from the centerline, however the amount of enclosed ion current places the divergence at the same location with and without the shield.

As mentioned previously, the errors for parameters significantly affected by flow have large errors due to the uncertainty associated with the actual flow into the chamber.

The calculated parameters in Table 8.3 show that the beam current only increased by 14.4% despite a 115% increase in discharge current. This is likely due to a change in the structure of the magnetic field inside the thruster. A decrease in discharge voltage along with the increase in discharge current shows that the HEMPT's axial electron impedance has significantly decreased. All three performance parameters, thrust, specific impulse, and total efficiency, showed a decrease with the addition of the shield. The following section will examine the reasons for this performance decrease and provide recommendations for future HEMPT testing.

8.3 RECOMMENDATIONS

The testing presented in the previous sections shows that while the particular shield that was implemented on the HEMPT did indeed fix the hollow plume issue, it significantly changed the magnetic field inside the thruster channel as well. During the design process, only the changes to the magnetic field outside the thruster were investigated. No consideration was given to the magnetic field reduction inside the channel, which was a mistake. The PPM system on the

HEMPT is designed for excellent plasma confinement and impedance of electrons upstream to the anode. The shield that was introduced provided a lower resistance path for the magnetic circuit around the outside of the thruster, thus lowering the magnetic field strength inside the thruster and causing the performance issue presented in Section 8.2.

In order to maintain the efficacy of the HEMPT's PPM system while attempting to reshape the plasma plume, the entirety of the magnetic field must be considered. Therefore three new shields were designed and modeled in MagNet with the goal of restoring the original magnetic field shape and strength inside the thruster channel while still reducing the field outside. While the original shield (Shield 2) provided the maximum reduction, a trade must be made between magnetic field reduction outside and limited change of the magnetic field inside.

A re-examination of the effect of Shield 2 on the magnetic field shows significant reduction in the magnetic field strength inside the thruster, as presented in Figure 8.6.

Three extra shields were considered in order to determine the best path forward. Shield 7 is the same as Shield 2, except the walls have been completely removed, leaving just the face of the original shield. Shield 8 keeps the shape of Shield 2 exactly the same, but cuts the thickness in half (0.1") everywhere. Shield 9 is also thin-walled like Shield 8, but cuts the wall length from the original 0.8" to a short 0.2". These three shields along with their relevant dimensions are presented in Figure 8.7 while the plots in Figure 8.8 present the radial and axial magnetic field strengths in the same manner as those in Chapter 4.

These new simulations show that a shield will no walls, like Shield 7, has

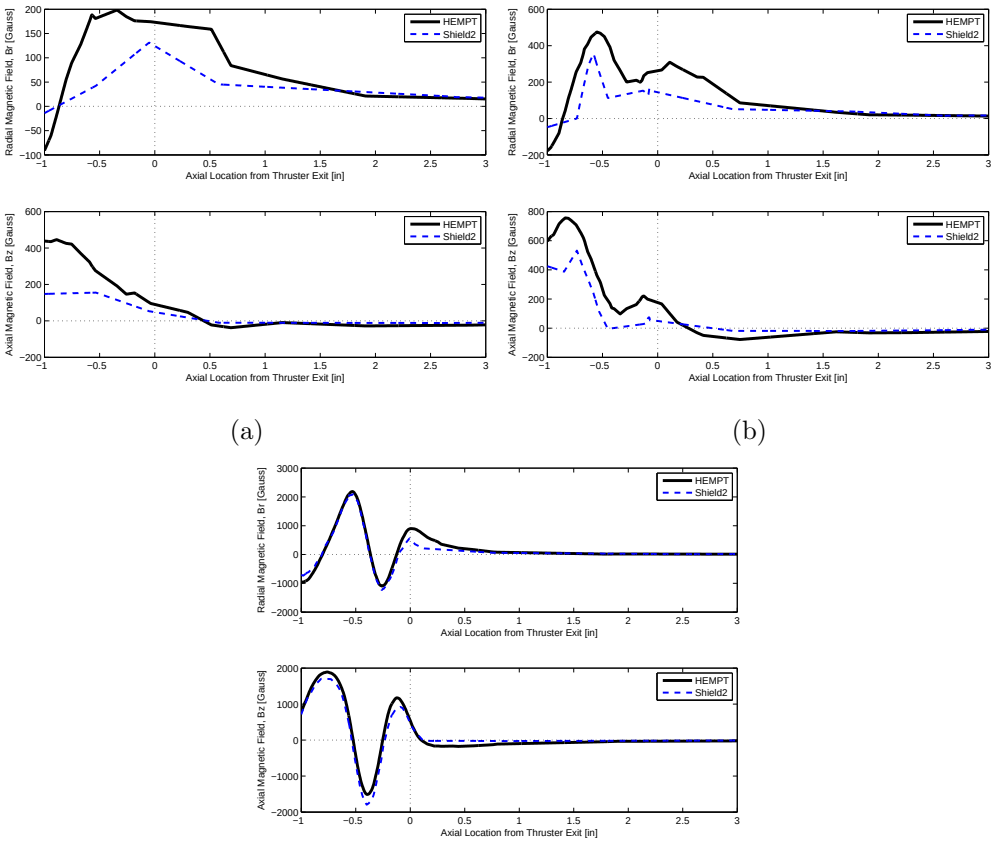

Figure 8.6: Shield 2 magnetic fields (a) along the thruster centerline (b) halfway between centerline and wall (c) along the channel wall, all evidence of significant B-field reduction inside the thruster channel

the smallest effect on the magnetic field strength inside the channel while still providing some reduction outside. This is most apparent in Figure 8.8 (a) and (b). This is likely because any sort of wall provides a lower resistance path outside the thruster, causing the magnetic field inside the channel to change, especially near the center of the thruster channel. The recommended change to the shield is then removal of the outer walls, as presented in Figure 8.9. No testing with this proposed shield change was conducted.

An investigation into exactly how much change inside the channel is acceptable for thruster operation should be part of the future work on this HEMPT.

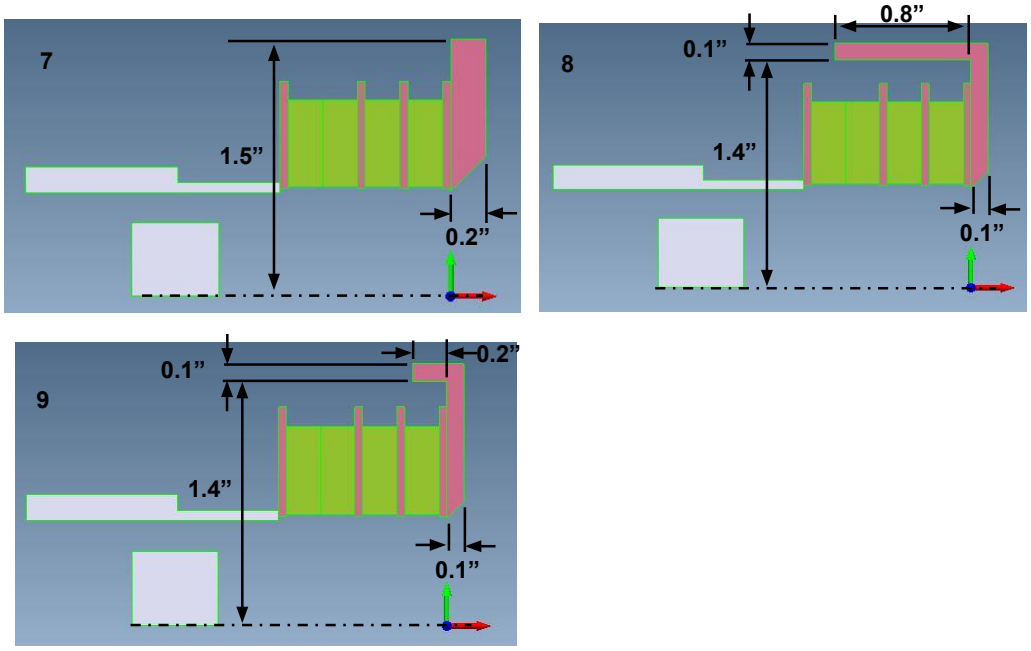

Figure 8.7: The three new shields that was examined post HEMPT testing along with their relevant dimensions

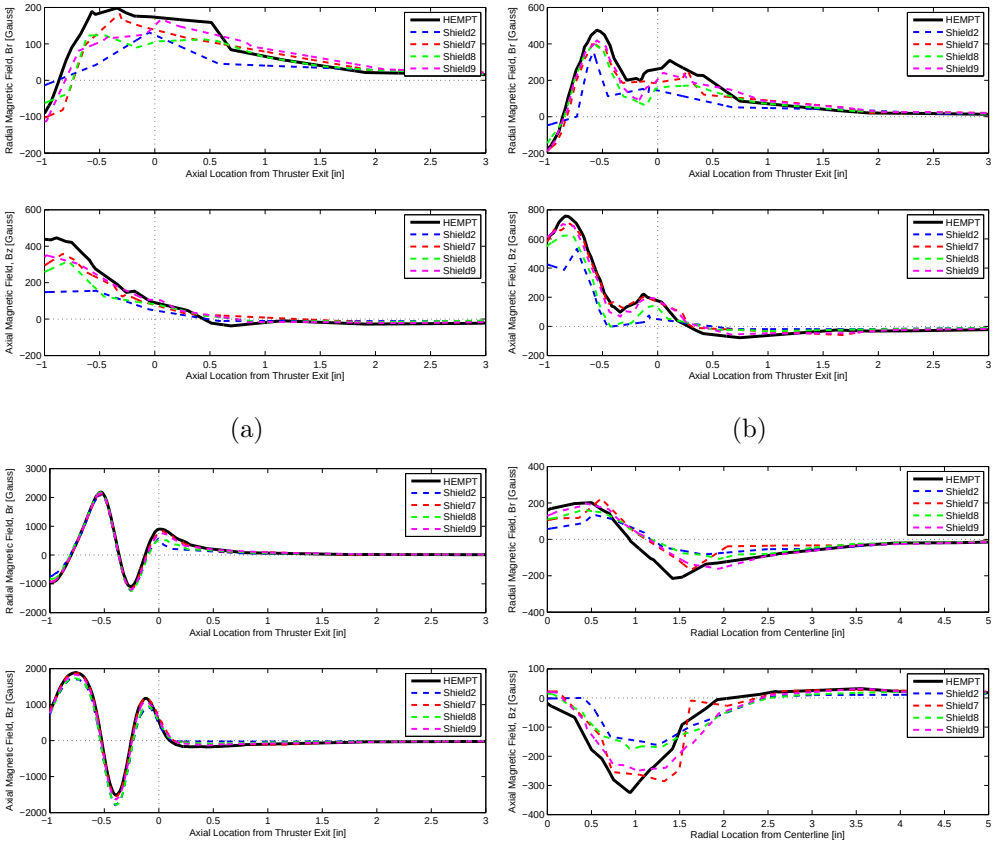

Figure 8.8: Shields 2, 7, 8, and 9 magnetic fields (a) along the thruster centerline (b) halfway between centerline and wall (c) along the channel wall (d) half-inch outside the thruster exit

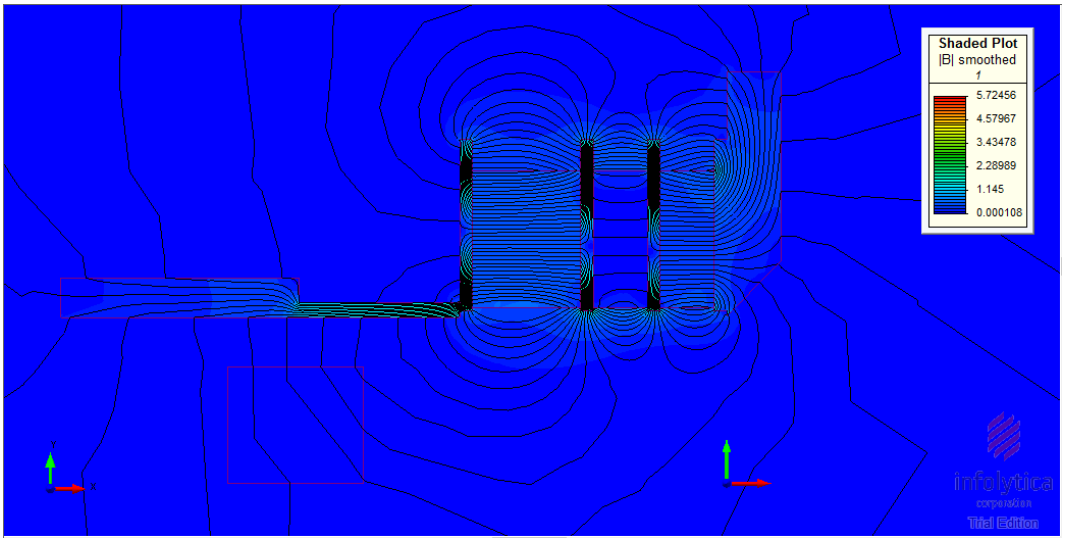

Figure 8.9: Recommended change to HEMPT shield design to be used in future testing

9. CONCLUSION

This thesis aimed to fix the hollow plume shape observed on a High Efficiency Multistage Plasma thruster through the implementation of an iron shield. The goal of the shield was to shunt much of the magnetic field that was present outside the HEMPT channel which was responsible for a reduced ion current along the thruster centerline. The strong magnetic field region outside the thruster pulled the ions outwards at large divergence angles. Before any testing took place, a shield was designed with the aid of a 2D magnetostatic modeling program to help mitigate this issue. The HEMPT's external magnetic field strength was examined for several different shield designs, and the shield with the maximum reduction in field strength was manufactured and implemented onto the thruster.

To determine the plume shape, an ion collection probe called a Retarding Potential Analyzer was built and utilized. This RPA was mounted on a linear probe drive that moved the probe across the center of the plume. Ion current was collected at set locations across the plume to build up the shape. This was done while operating the HEMPT with and without the shield to determine the change in plume shape as a result of the implemented iron shield.

Testing of the laboratory HEMP-thruster with implemented shield yielded some unexpected results. The shield did fix the HEMPT's hollow plume, but at a cost to the overall performance of the thruster; decreases in thrust, specific impulse, and efficiency all resulted from this design. The shield decreased

the magnitude of the radial magnetic field cusps near the center of the thruster channel, allowing electrons to stream to the anode and significantly increasing the discharge current while lowering the discharge voltage and consequently the beam voltage, an important value in thrust calculations.

This result is due to the focus that was placed on changing the outer magnetic field without regard for what happened inside the thruster channel during the shield design process. A broader view of the entire thruster magnetic field must be utilized in the future to prevent this adverse effect. A suggestion has been made to remove the walls of the current shield, however testing must be performed to validate whether this design change provides the expected result of removing the hollow plume and restoring or increasing the performance of the thruster.

9.1 FUTURE WORK

An investigation must also be initiated to determine why the RPA showed such large collected current at high retarding potentials, as well as why a delay exists in the collection of current. It is likely the first of these is a result of the second. This unfortunate phenomenon required that all RPA curves be discarded, requiring the estimation of an important performance parameter. It would be beneficial for future projects to use several different probes, like a Faraday probe or ion saturation probe, many of which can be manufactured at Cal Poly, in order to provide more accurate measurements of thruster parameters.

This thesis was almost purely experimental, consisting of placing a shield on the thruster and determining the results of this change through testing. Future work should include a theoretical analysis of the magnetic field changes due to the shield and its parameters. This should include forming relationships between

thicknesses and placements of shield parts and the corresponding changes these have on the structure of the magnetic field. Plasma models can also be utilized with different shield designs to determine the effects of shielding on the plume shape without requiring facilities in which to test. This thesis also only focused on a single shield design with small variations. A different design, perhaps with the shield walls extending forward rather than back around the thruster should also be examined.

Before future testing, a detailed calibration of the flow and pressure measurement system, as well as vacuum pumping speed should be performed. A properly calibrated system will allow accurate calculations of thruster performance and will hopefully remove the need to add an arbitrary correction factor to the flow calculation parameters.

Through this thesis, the current largest vacuum chamber has been readied for future thruster testing, which will hopefully continue to be used to examine this HEMPT as well as the other electric propulsion thrusters available at Cal Poly.

BIBLIOGRAPHY

[1] Hall Thruster Research Group: About Hall Thruster. Website. http://www.al.t.u-tokyo.ac.jp/hall/en/projects.html.

[2] Jet Propulsion Laboratory: Electric Propulsion. Website. http://sec353ext.jpl.nasa.gov/ep/multimedia.html.

[3] NASA Glenn Research center. Website. http://www.nasa.gov/centers/glenn/about/fs08grc.html.

[4] *OMEGA FMA-A2300 Massflow Meter User's Guide.*

[5] D. Courtney, P. Lozano, and M. Martinez-Sanchez. Continued Investigation of Diverging Cusped Field Thruster. In *AIAA/ASME/SAE/ASEE Joint Propulsion Conference*, number AIAA 2008-4631, 2008.

[6] C. L. Enloe and J. R. Shell. Optimizing the Energy Resolution of Planar Retarding Potential Analyzers. *Review of Scientific Instruments*, Vol. 63(2), February 1992.

[7] J. C. Gayoso, Y. Raitses, and N. J. Fisch. Cathode Effects on Operation and Plasma Plume of the Permanent Magnet Cylindrical Hall Thruster. In *32nd International Electric Propulsion Conference*, number IEPC-2011-247, 2011.

[8] D. Goebel. Personal Communcation, November 2013.

[9] D. Goebel and I. Katz. *Fundamentals of Electric Propulsion: Ion and Hall Thrusters*. JPL Space Science and Technology Series. John Wiley & Sons, Inc., 2008.

[10] H.-P. Harmann, N. Koch, and G. Kornfeld. Low Complexity and Low Cost Electric Propulsion System for Telecom Satellites Based on HEMP Thruster Assembly. In *International Electric Propulsion Conference*, number IEPC-2007-114, 2007.

[11] R. R. Hofer. Development and Characterization of High-Efficiency, High-Specific Impulse Xenon Hall Thrusters. Ph.D, University of Michigan, 2004.

[12] K. K. Jameson. Investigation of Hollow Cathode Effects on Total Thruster Efficiency in a 6 kW Hall Thruster. Ph.D, UCLA, 2008.

[13] L. B. King. Transport-Property and Mass Spectral Measurements in the Plasma Exhaust Plume of a Hall-Effect Space Propulsion System. Ph.D, University of Michigan, 1998.

[14] D. W. Knapp. Implementation of a 1/4 inch Hollow Cathode into a Miniature Xenon Ion Thruster (MiXI). M.S., California Polytechnic State University, 2012.

[15] N. Koch, H.-P. Harmann, and G. Kornfeld. Development & Test Status of the Thales High Efficiency Multistage Plasma HEMP Thruster Family. In *International Electric Propulsion Conference*, number IEPC-2005-297, 2005.

[16] N. Koch, H.-P. Harmann, and G. Kornfeld. Status of the THALES High Efficiency Multi Stage Plasma Thruster Development for HEMP-T 3050 and HEMP-T 30250. In *International Electric Propulsion Conference*, number IEPC-2007-110, 2007.

[17] G. Kornfeld, N. Koch, and G. Coustou. First Test Results of the HEMP Thruster Concept. Technical report, Thales Electron Devices GmbH, 2003.

[18] G. Kornfeld, N. Koch, and H.-P. Harmann. Physics and Evolution of HEMP-Thrusters. In *International Electric Propulsion Conference*, number IEPC-2007-108, 2007.

[19] Y. Raitses, J. C. Gayoso, and N. J. Fisch. Effect of Magnetic Shielding on the Plasma Plume of the Cylindrical Hall Thrusters. In *32nd International Electric Propulsion Conference*, number IEPC-2011-175, 2011.

[20] Y. Raitses, J. C. Gayoso, E. Merino, and N. J. Fisch. Effect of the Magnetic Field on the Plasma Plume of the Cylindrical Hall Thruster with Permanent Magnets. In *AIAA/ASME/SAE/ASEE Joint Propulsion Conference*, number AIAA 2010-6621, 2010.

[21] R. Shastry, R. R. Hofer, B. M. Reid, and A. D. Gallimore. Method for Analyzing ExB Probe Sprectra from Hall Thruster Plumes. *American Institute of Physics*, 2009.

[22] G. Sutton and O. Biblarz. *Rocket Propulsion Elements*. John Wiley & Sons, Inc., 8th edition, 2010.

A. LESSONS LEARNED

This thesis provided many difficulties and challenged, but was an excellent learning experience. Some of the lessons learned will be detailed here.

The basic design of the magnetic shield was determined early on based mostly on previous work done with the CHT at PPPL. This thruster used a specific shape for the shield, and that shape was carried over into this thesis. This prevented original and out-of-the-box thinking about new ways to approach a shield, which could have aided in the design and allowed for a better and less detrimental shield with regards to HEMPT performance. Getting stuck into a specific design without thinking about other approaches should be avoided.

Another important lesson was not to be too narrow minded during a design process. While designing the shield, the data was present that the chosen shield could have detrimental effects on thruster performance, as evidenced when taking a second look at the magnetic field inside the thruster while the shield was implemented. Unfortunately, focus was placed solely on the magnetic field outside the channel. A broader view of the magnetic field as a whole could have saved time as well as resulted in a more effective shield for the thruster.

There are many different types of plasma probes available, many of which can provide similar information. Perhaps more thought should have gone into the probe selection process. A ion saturation probe, Faraday probe, or other

probe types would have provided the same picture of the plume while having a simpler set up. The RPA required several power supplies and feedthroughs into the chamber, and both of which were limited and caused issues during testing.

One of the most frustrating parts of this thesis was waiting for the chamber to pump down enough to begin testing. This took approximately 3 days on average, meaning each time something was incorrect in the setup, half a week of testing was wasted, leading to a total testing time of about 2 months. Everything needs to be double and then triple checked to ensure proper setup to prevent time from being wasted unnecessarily, especially if a pressing schedule is a factor. Originally, only about 3 to 4 weeks of testing was scheduled for this project. Not only did testing take about 8 weeks, it also didn't even begin until about 4 months after the original testing was scheduled. Make sure to include a large margin for testing, many things that have not been thought of can, and most probably will, go wrong.

One important lesson learned was ensure proper insulation of high voltage wires in the chamber. During the very first HEMPT test, the discharge line in the chamber (200V), was only isolated from the plasma by the standard insulation of a 14 AWG wire. This wire became extremely hot near the anode connection, burning off some insulation and exposing a part of the wire. The plasma was immediately attracted straight from the cathode to this exposed wire, bypassing the thruster. This meant most of the plasma was created outside the wire. The rest of the insulation on the discharge line was burned off, intensifying the problem. This problem was fixed by wrapping A LOT of insulation (Kapton tape and Teflon sheets) around this wire. This was then applied to all other high voltage lines in the chamber. It is important to know which areas require special preparation before thruster testing.

The hollow cathode was often quite tricky to strike, requiring two power supplies in parallel for the keeper. High current diodes must be placed the proper places in between these supplies to protect them. It is often a good idea to place several diodes in each location as a redundancy. Often, diodes would be destroyed from the high voltage and current between the two supplies, and backup diodes were there to ensure the power supplies were still protected.

Another major lesson learned is the susceptibility of the chosen motor and motor drive circuitry to interference and noise in the system. The microcontroller and motor drive board were placed in close proximity to the cathode keeper and discharge supplies based on convenience. These supplies were operated at high voltages and currents, which seemed to give the probe control circuitry a lot of trouble. Acrylic and foil wrapped around lines and circuit components attempted to shield these sensitive electronics from this interference however in the future, it would likely be best to move these components to a different physical location, far away from the other power supplies.

B. PROCEDURES

B.1 FULL HVEC HIGH VACUUM PROCEDURE, CRYO PUMP OFF

1. Turn on compressed air supply at wall
2. Turn on System Power
3. Turn on Mechanical Pump
4. Turn on Chamber Rough
5. Rough out chamber to a low pressure, i.e. 50 mTorr
6. Turn on Pressure Override
7. Turn on Rough Interlock
8. Open Gate Valve
9. Allow pressure to pump down below 50 mTorr
10. Turn on the Compressor
11. After 30-40 minutes, shut the chamber rough (temp 150 Kelvin)
12. Turn off the Mechanical Pump
13. Turn off Rough Interlock

14. Turn on Pressure Interlock
15. Turn off Pressure Override
16. Allow temperature to drop to 17 Kelvin in cryo
    (a) Ensure the pressure does not rise above 150 mTorr during cryo cool-down period
17. Once convectron gauge zeros, press Ion Gauge 1 button to turn on the ion gauge

B.2 SHORT HVEC HIGH VACUUM PROCEDURE, CRYO PUMP ON

1. Turn on Mechanical Pump
2. Turn on Chamber Rough
3. Allow pressure to drop below 50 mTorr
4. Close Chamber Rough
5. Turn off Mechanical Pump
6. Turn on Pressure Interlock
7. Open Gate Valve
8. Once convectron gauge zeros, press Ion Gauge 1 button to turn on ion gauge

B.3 HIGH VACUUM TOTAL SHUT DOWN PROCEDURE

1. Turn off Ion Gauge 1

2. Shut Gate Valve

3. Turn off Pressure Interlock

4. Turn off Compressor

5. Open the Vent Valve

6. Let the chamber vent to ambient pressure (760 Torr)

7. Close the Vent Valve

8. Turn off the Compressed Air supply at wall

9. Turn off the System Power

B.4 HOLLOW CATHODE TESTING PROCEDURE

1. Clean all equipment with Acetone and hook up propellant lines to the cathode

2. Attach electrical connectors to the power supplies, cathode, and anode (see electrical schematic)

   (a) Positive lead of heater supply attaches to wire out the back of cathode

   (b) Negative lead of heater supply attaches to common ground

   (c) Positive lead of keeper supply attaches to cathode keeper

   (d) Negative lead of keeper supply attaches to chassis of hollow cathode stand and to common ground

   (e) Positive lead of anode supply attaches to the anode

   (f) Negative lead of anode supply attaches to common ground

(g) Ground the chamber to common ground

3. Pump the chamber down to an acceptable base pressure (less than $5.0 \text{x} 10^{-6}$ Torr) using the procedure in Appendix B.1 or B.2 as needed.

4. Open all propellant lines to the vacuum and allow sufficient time for them to be evacuated and the pressure to equalize again

5. Turn on heater supply to 5-6 A for 25 minutes

6. Turn on the Xenon gas supply

7. Set the stainless steel regulator to 25 psi

8. Adjust the flow control to obtain 5 sccm Xenon flowing to the cathode

9. Turn on the keeper supply and continue increasing the voltage until you achieve current pull. Set to 2 A.

10. Shut off the heater supply

11. Turn on the anode supply to 30 V

12. Adjust flow rate to cathode as necessary for testing purposes

13. Test until ready to shut everything down

14. Shut off the anode supply

15. Shut off the keeper supply

16. Shut off the gas flow to the cathode

17. Let the cathode cool down for 3-4 hours until ambient temperature has been reached

B.5 THRUSTER TESTING PROCEDURE

1. Clean all equipment with Acetone and hook up propellant lines to thruster and cathode
2. Attach all electrical connections to power supplies, thruster, and cathode (see electrical schematic)
   (a) Positive lead of discharge supply attaches to copper connector on the HEMPT propellant line
   (b) See Appendix B.4 for Hollow Cathode hook-up procedure
3. Pump the chamber down to an acceptable base pressure (less than 5.0×10^{-6} Torr) using the procedure in Appendix B.1 or B.2 as needed
4. Open all propellant lines to vacuum and allow sufficient time for them to be evacuated and the pressure to equalize
5. Close shut off valve to thruster and hollow cathode
6. Light hollow cathode per Appendix B.4 steps 5 - 10, except also open the shut off valve to thruster and adjust Xenon flow to 5 sccm at the same time as cathode flow
7. Once cathode is lit, turn the voltage on the discharge supply up to 200 V
8. Adjust discharge supply voltage as necessary depending on testing
9. Perform testing and plume measurements
10. When done, shut off all power supplies and the gas flow to the system

11. Let the cathode and thruster cool down for several hours until ambient temperature has been reached